SBUF

ID: 13745

SKANSKA

Byggautomation – Utmattningshållfasthet hos robotsvetsad armering

Alexander Kjellgren

2019-09-10

Fatigue Evaluation of Robot Welded Reinforcement Bars

Alexander Kjellgren

Division of Structural Engineering
Faculty of Engineering, LTH
Lund University, 2019

Avdelningen för Konstruktionsteknik
Lunds Tekniska Högskola
Box 118
221 00 LUND

Division of Structural Engineering
Faculty of Engineering, LTH
P.O. Box 118
S-221 00 LUND
Sweden

Fatigue Evaluation of Robot Welded Reinforcement Bars

Utmattningsutvärdering av robotsvetsade armeringsjärn

Alexander Kjellgren
2019

Rapport TVBK-5272
ISSN 0349-4969
ISRN LUTVDG/TVBM-19/5272(72)
Examensarbete
Handledare: Eva Frühwald Hansson (LTH), Lars Pettersson (Skanska), Anna Björklund (Skanska).
Juli 2019

Abstract

In the automatization of the infrastructure engineering trade, large time savings during construction may be obtained. One possibility is prefabrication of reinforcement units on the construction site where assembling is executed by industrial robots. The reinforcement unit needs to obtain sufficient stiffness in order to keep together during the lifting sequence into the mold. Welding is an option to achieve stiffness to the unit, however welding of reinforcement bars come with reduction in fatigue strength.

Material fatigue was examined in order to develop an understanding of differences between static and cyclic loading as well as available approaches on the subject.

Present design regulations in Eurocode 2 are conservative regarding welding and fatigue issues and perhaps robot welding outperform design S-N curves. The standard was written in the 1980'ies and scientific support for fatigue of reinforcement bars were available up to approximately $2 \cdot 10^6$ cycles. Longer fatigue life, are hence pragmatic guesses as well as curve inclination after $2 \cdot 10^6$ cycles.

An experimental program was carried out where 23 welded reinforcement bars were subjected to fatigue loading until failure. The welds were non load-carrying and performed by industrial robots with a MAG135 method. Stress ranges of 280, 176, 164 and 148 MPa were selected and fatigue lives between approximately $400 \cdot 10^3$ and $800 \cdot 10^3$ cycles were noted.

It can be concluded that for the selected stress ranges, MAG135 robot welding performs in good agreement with design S-N curves. No benefits were seen as to these stress ranges. However, this may change regarding lower stress ranges since fatigue lives longer than $2 \cdot 10^6$ cycles are pragmatic assessments in the standard.

Finally, fracture surfaces were studied with optical microscope in an attempt to capture different fatigue stages, described in the literature. Fatigue fracture surfaces are different compared to static loading fracture and pictures highlighting the differences were produced.

Sammanfattning

Automatisering av anläggningsbranschen kan spara mycket produktionstid. En möjlighet är prefabricering av armeringsenheter på arbetsplatsen där sammansättningen kan göras av industrirobotar. Armeringsenheten måste vara tillräckligt styv för att kunna lyftas ner i gjutformen. Svetsning är ett alternativ för att uppnå tillräcklig styvhet, dock innebär svetsning av armeringsjärn att utmattningshållfastheten reduceras.

Materialutmattning undersöktes för att utveckla en förståelse för skillnader mellan statisk och cyklisk belastning samt tillgängliga angreppssätt av ämnet.

Nuvarande bestämmelser i Eurocode 2 är konservativa när det gäller svetsning av armeringsjärn där det uppstår utmattningslast men eventuellt kan robotsvetsning överträffa nuvarande S-N kurvor. Normen skrevs under 1980-talet och vetenskapligt underlag, vad gäller utmattningsliv i cykler, var ansenligt upp till ungefär $2 \cdot 10^6$ cykler. Utmattningsliv längre än $2 \cdot 10^6$ cykler utgörs av pragmatiska bedömningar, så också kurvlutning efter $2 \cdot 10^6$ cykler.

En serie av experiment utfördes där 23 svetsade armeringsjärn utmattningslastades till brott. Svetsarna var icke lastbärande och utförda av industrirobotar med svetsmetod MAG135. Spänningsvidder om 280, 176, 164 och 148 MPa valdes och utmatningsliv mellan ungefär $400 \cdot 10^3$ och $800 \cdot 10^3$ cykler noterades.

Sammanfattningsvis uppvisade provkropparna provningsresultat i enlighet med normen. Robotsvetsningen uppvisade inga fördelar vid dessa spänningsvidder. Emellertid, kan lägre spänningsvidder ge bättre resultat eftersom dessa livslängder består av pragmatiska bedömningar då normen skrevs.

Avslutningsvis, studerades brottytor med optiskt mikroskop i ett försök att fånga olika utmattningssteg, som beskrivs i litteraturen. Utmattningsbrottytor är utmärkande jämfört med brottytor från statisk belastning och bilder på detta har tagits fram.

Preface

This master's thesis concludes five year studies for a degree of Master of Science in Civil Engineering. The thesis has been performed at the Division Structural Engineering at Lund University in cooperation with Skanska, where a majority of the work has been done.

I would like to thank my supervisor at Skanska Lars Pettersson for his help during the work and especially his enthusiasm for developing and improving technical solutions has been very inspiring. Furthermore, I am very grateful of the help from Anna Björklund at Skanska who always had time for questions and made me feel most welcome at Skanska. I also wish to extend my gratitude to my supervisor at LTH, Eva Frühwald Hansson for the valuable comments on the report during this semester. Finally, I am thankful of the help from Per-Olof Rosenkvist who executed the fatigue testing.

The work of establishing background to present fatigue sections in Eurocode had not been possible without the help from several persons who could point me in the right direction, especially Lennart Elfgren, LTU. A special thanks to Konrad Zilch in Münich for sending me background documents to present design standard.

Specimen production was performed at CH-industry in Eskilstuna and they never demanded anything in return. I am most greatful of the help from CH-industry and especially David Diaz who produced specimens and answered questions concerning welding.

I would like to thank my family and friends for all their love and support throughout my education. Especially Jakob d.d.S. Ingesson from who I developed a passion for applied mathematics, structural mechanics and structural engineering. We have had many challenging discussions with the sole purpose of annihilating each other's arguments.

Finally, to my great love Matilda Abrahamsson, who has endured my endeavor to a higher education with unlimited love and support. You make the best out of me.

List of Figures

List of Tables

Nomenclature

ΔK	Stress intensity factor
$\Delta\sigma$	Stress range
$\Delta\sigma_{Rsk}$	Resisting stress range at N^* cycles
$\Delta\sigma_{s,Ec}$	Stress range from appropriate load model
$\Delta\sigma_{s,equ}$	Equivalent damage stress range
$\gamma_{r,pl}$	Resolved plastic shear strain
λ_s	Damage equivalent factor
ϕ	Reinforcement bar diameter
σ_a	Stress amplitude
$\sigma_{\max}$	Maximum stress of a loading cycle
σ_{mean}	Mean stress of a loading cycle
$\sigma_{\min}$	Minimum stress of a loading cycle
τ_r	Resolved shear stress
τ_s	Saturated shear stress
C	Material constant, Basquin equation, ordinate crossing
da/dN	Crack propagation rate
e	Residual between predicted and tested fatigue life
$F_{\max}$	Maximum force of a loading cycle
$F_{\min}$	Minimum force of a loading cycle
k	Curve inclination in S-N diagram
m	Material constant, Paris law
N^*	Number of cycles at S-N curve inflection point
N_f	Fatigue life
$N_{f,i,\text{predic},5\%}$	5% fractile to predicted fatigue life from linear regression

$N_{f,i,\text{predic}}$ Predicted fatigue life from linear regression

R Stress ratio

R^2 Correlation coefficient

s Standard deviation

Contents

Chapter 1

Introduction

Fatigue evaluation for structures of reinforced concrete is mainly a concern for bridges and offshore installations since high live load levels are anticipated. Material fatigue in infrastructure engineering is in all essence originating from varying live loading causing *stress ranges* to appear in different elements. The load situation is however hard to anticipate since future traffic volumes never are known, which render the number of loading cycles and corresponding stress ranges unknown [1]. A typical bridge is designed for a technical life time of 120 years which in practice would imply a total amount of stress cycles well above 10^9 cycles for a bridge exposed to high frequency heavy traffic. When fatigue design of reinforced concrete is considered, welded reinforcing steel is usually a limiting factor in design.

The main topic herein, is welded reinforcement bars (rebars) and associated fatigue behaviour when industrial robots have performed the welding. A detailed background of the thesis is presented in the next section as to the automation process in infrastructure engineering. Furthermore, scope with limitations are introduced to confine the subject to a graspable size. Finally, a chapter disposition is briefly presented in order to obtain an overview of the thesis.

1.1 Background

Swedish tradition regarding the production of reinforcement units such as meshes and cages, concerning in-situ cast concrete, is well-established. When longitudinal and transverse reinforcement bars are connected to ensure that the bars are kept together during concreting, a simple *rebar wire tying* is conducted, which in practice means that the crossing of two bars is lashed together by a small wire. In infrastructure engineering, in-situ casting is more or less standard procedure. The process of constructing the reinforcement unit is time consuming and demanding for the skilled workers. This brings out the question whether this part of the casting process can be automated. It turns out that it might be possible to use industrial robots in the construction of reinforcement units. However, to use industrial robots implies that welding of the reinforcement crossings becomes of interest since this may be beneficial in the automated production. If reinforcement units are prefabricated (prefab) on site and lifted into the mold

before concreting, the units need stability and rigidity, properties which do not exist when *rebar wire tying* is used. Welding provides sufficient stability to the reinforcing unit during lifting phases.

The overall possibility to use welded connections between reinforcement bars is in present day highly limited due to low reference fatigue strength values in the standard. Welding frequently affects the reinforcement bars, whereon it is hard to evaluate the remaining strength in the bars. This results in the low reference fatigue strength values in the standard, i.e. $\Delta\sigma_{Rsk}$, see Section 2.6.1. It is thus not the weld itself that is interesting, but the remaining strength of the rebar subjected to welding treatment. Following the standard entails in practice untenable design situations and welded rebars in fatigue prone structures are in reality rarely used.

In order to facilitate the use of welding in the manufacturing of reinforcement units, it should be concluded that present reference fatigue strength values are not representative for welds performed by industrial robots. A probability exists that industrial robots can perform welding in such a way that the reinforcement bars are kept sufficiently unaffected.

Developments of an automated production of reinforcement units have begun. In short, the idea is to establish a reinforcement unit installation station on site, consisting of a cutting- and bending machine and three robot arms mounted on overhead cranes. The cutting- and bending machine prepares reinforcement bars whereon robots proceed by assembling the prepared reinforcement bars with tying or spot weld to desired units. A reinforcement unit is subsequently lifted into the mold whereat concreting is initiated. Figure 1.1 is a sketch of the intended reinforcement station.

Skanska (construction company) and *ABB* (automation company) have successfully constructed reinforcement units through the above process, however only in prototype environment and on small scale. The concept of a *manual* reinforcement construction station on site has also been tested in practice with promising results. An area where reinforcement was assembled into units with welding and then lifted into the mold was established on full scale at a Skanska construction site. The finished structure was however designed with low fatigue loading which enabled welding of reinforcement units.

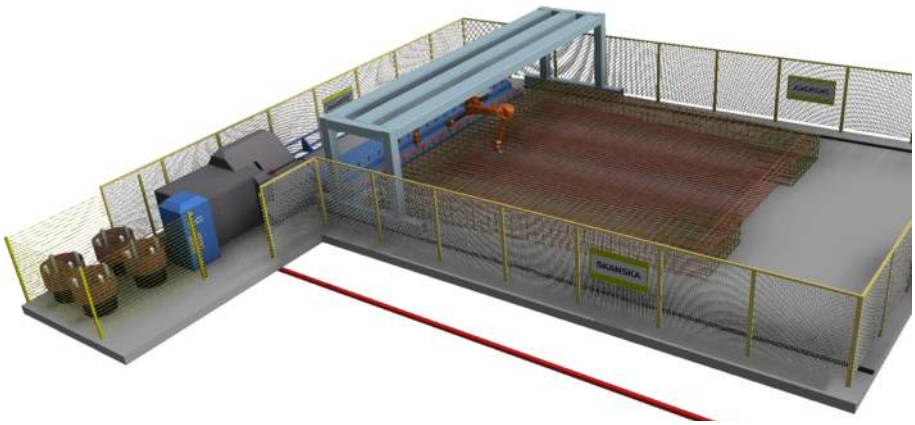

Figure 1.1: Schematic view of an intended reinforcement unit construction station.

A logical next step is to evaluate fatigue properties of reinforcement bars influenced by welding, where welding has been performed by industrial robots. Furthermore, the results should be compared to the present design standard, i.e. *Eurocode 2* (EC2) [3a].

1.2 Scope

Fatigue of materials and structures has become a vast area of research and several sub domains can be defined under the concept of fatigue. The tested and evaluated reinforcement bars are dealt with as *as received bar* thus influence from concrete is completely disregarded. Studies imply safe side when reinforcement bars are tested in air as test results show lower fatigue strength when compared to bending tests of reinforced concrete beams [1, 2d]. Bond breaking fatigue between concrete and reinforcement and any other positive or negative interaction effects are thus not covered.

Fatigue performance of reinforcement bars differ when bending and axial fatigue are compared; however, bending fatigue is left out and only uniaxial tension fatigue is evaluated.

Questions of corrosion effects on fatigue performance is of high concern when service life assessments are conducted on in-service bridges. The tested reinforcement bars herein, have by a small extent been corroded, see Figure 1.2, since all were received from a construction site. By extension, all reinforcement bars were not identical and no pre-conditioning was performed on any surfaces implying that some differences between starting conditions are expected. However, since the reinforcement bars are as new as possible, an assumption of negligible effects from small corrosion is reasonable and also entails plausible situations when it comes to in-situ cast reinforced concrete, where minor corrosion is expected. Corrosion fatigue will not be dealt with further.

Although the fatigue life of reinforcement bars is of high importance, attention is also necessary for the concrete itself when design is performed. Fatigue of concrete is not covered and only the reinforcement bars are considered.

Pre- and post tensioning of concrete structures are also an interesting subject regarding fatigue. Design standards, e.g. *Eurocode 2* [3, 4] and fib Model Code 2010 [5], distinguish between tensioned reinforcement and "traditional" reinforcement. Pre- and post tensioned reinforcement is disregarded hereinafter in this study.

Considering design codes as *Eurocode 2* (EC2) [3, 4] or fib Model Code 2010 (MC2010) [5], bending of reinforcement bars clearly has a negative impact on

Figure 1.2: Overview of a specimen showing the *as received* status with limited corrosion.

fatigue life. Only straight bars are investigated and bent bars are not discussed further.

In Sweden, design of reinforced concrete structures applied in infrastructure engineering, are governed by numerous standards and regulations beyond EC2. *TRVFS* [6], *TRVK* [7, 8] and *TRVR* [9, 10] are important regulations and function as amendments to the *Eurocode* design standard. In the analysis of the results, only EC2 will be considered since it is the most essential standard regarding fatigue design of reinforced concrete structures.

In literature and design, a distinction is made between load-carrying and non load-carrying welds. The purpose of the welds is to keep the reinforcement unit together during concreting and perhaps sustain some minor accidental mistreatment during construction. Once concreting is finished the welds are no longer needed. With this in mind, the welds are treated as non load-carrying in design calculations and the interesting part is not the weld itself, but how the welding process affects the longitudinal rebar.

1.3 Disposition

An outline of chapter content is briefly treated next.

Chapter 1 - Introduction

An overview of the thesis is presented which should provide an overall glimpse to the project. Project background is described together with scope and thesis disposition.

Chapter 2 - Theory

The concept of material fatigue is introduced regarding governing parameters and different fatigue approaches. Furthermore, crystalline microstructures are scrutinized as to material damage in general and the concept of dislocation movement. Thence metal fatigue, in connection to important microstructural characteristics are discussed concerning specific material damage from cyclic loading. The general fatigue stages, *crack initiation*, *crack propagation* and *failure*, are subsequently treated whereon differences in static and cyclic loading are presented. Next, reinforcing steel microstructure is treated in relation to fatigue and the implications from welded rebars are also introduced. Previous literature and papers deemed relevant, are integrated all through Chapter 2 when necessary. Finally, governing design regulations in EC2 are presented with relevant parameters to experimental testing herein.

Chapter 3 - Method

Welded specimens were tested in fatigue and the experimental procedure is described in detail regarding specimen configuration, steel material and loading conditions. Selected and tested stress ranges are presented and succeeding statistical analysis of the test results is also shown as to linear regression and 5% lower tolerance limit. The usage of an optical microscope is briefly discussed where fracture surfaces were studied.

Chapter 4 - Results

The different tested stress ranges with corresponding fatigue life are presented graphically and in tables. Fracture surfaces from selected specimens are observed both with ordinary camera and from optical microscope.

Chapter 5 - Discussion

An overall discussion of the test results is carried out. The theory is interweaved with the test results and final conclusions are presented.

1.4 Objectives

A profound investigation as to *background* and *selection* of the present reference fatigue strength values will be the start of the thesis. To thoroughly clarify the intent, assumptions, underlying theory and previous test results from which present reference fatigue strength values are based is of importance. The outcome from the background to the fatigue sections in EC2, might be insightful facts when proceeding to the next step.

Reinforcements bars with transverse rebars connected by welds performed by industrial robots will be tested uniaxially in fatigue until failure. The results will be compared to present reference fatigue strength values and the outcome will indicate whether present reference fatigue strength values are representative for welds performed by industrial robots.

The results from laboratory testing are to be evaluated with the objective of introducing reference fatigue strength values that are more suitable for welds performed by industrial robots.

1.5 Approach

Initially a literature study along with contact with authorities and universities will be conducted in order to establish background and selection of the current reference fatigue strength values.

Laboratory testing of robot-welded connections as to crossings of reinforcement bars will be performed. The reinforcement bars will be tested uniaxially in fatigue until failure. A specimen will be a simple structure consisting of two reinforcement bars where one has been welded to the other as a transverse bar, see Figure 1.2. The important point is that the reinforcement bars, which will be tested uniaxially, have been altered by the welding.

The data from the testing will consequently be evaluated in order to obtain recommendations for reference fatigue strength values for welding performed by industrial robots.

Chapter 2

Theory

Material fatigue is studied in great extent, especially for ductile solids as metals. The field of fatigue is ascribed the work of pioneer *August Wöhler* who studied fatigue performance of railway locomotive axles in the middle of the 19th century. Wöhler discovered damage to the axles which could not be explained from static loading and later found differences to material damage from static contra cyclic loading. Since then, the research has increased drastically and fatigue design of fatigue prone structures is today always under consideration. However, fatigue design approaches and fundamental assumptions have not developed that much since the work of Wöhler.

The available approaches for fatigue performance evaluation of a structural component will be addressed in forthcoming sections as well as relevant parameters for fatigue loading endurance. Furthermore, fatigue of metals and the importance of microstructural properties are also dissected which pave the way for a general description of metal fatigue life domains as to microstructural damage, crack initiation and crack propagation. Rebar microstructure and its implications for rebar fatigue strength are the next subject which also will be narrowed down to some scrutinizing over fatigue performance of weld affected steel and rebars and suitable testing methods as of the same. Background to present design standard, *Eurocode 2* (EC2) [3a], has been examined as far as possible where some selection of design parameters are reviewed. Finally, a brief overview over the chosen statistical evaluation method of the test series as to linear regression is discussed.

2.1 Fatigue Life Parameters

When fatigue, in relation to a components expected life span is considered, the *fatigue life*, N_f, is a fundamental quantity which is the number of cycles at a *constant* stress range that a component can endure before failure. Several parameters influence the fatigue life of materials and are in general *stress range*, *stress ratio*, *mean stress*, *discontinuities* and *temperature*, as summarized in the list below [1, 11b].

- Stress range, $\Delta\sigma$
- Stress ratio, R

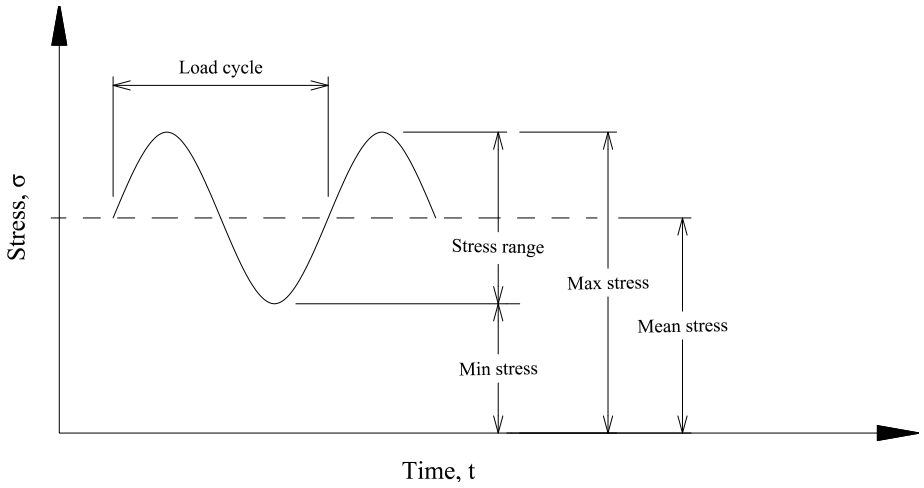

Figure 2.1: Definitions of fatigue parameters visualized in a stress over time diagram. Inspired by [12].

- Mean stress, σ_{mean}
- Discontinuities
- Temperature

These parameters will be discussed further in forthcoming sections, see sections 2.1.1, 2.1.2, 2.1.3, 2.1.4 and a graphic interpretation of one load cycle, stress range, stress ratio and mean stress is shown in Figure 2.1.

2.1.1 Stress Range

The difference between maximum and minimum stress is the stress range, $\Delta\sigma$, and is calculated according to (2.1). By definition of cyclic loading, the stress range is very important when fatigue performance is considered and occasionally the cyclic loading is expressed as stress amplitude, σ_a, which also is defined in (2.1). It should be emphasized that within the very concept of material fatigue, a cyclic loading and by extension an acting stress range is the definition of fatigue loading.

$$\Delta\sigma = \sigma_{\max} - \sigma_{\min}; \qquad \sigma_a = \frac{1}{2}\Delta\sigma \tag{2.1}$$

Since the first discovery of material fatigue by Wöhler, a fundamental difference between cyclic and static loading is the stress range which is alternating stress between a maximum and a minimum. The cyclic loading causes specific material damage which is different from static loading, see Section 2.4.4.

2.1.2 Stress Ratio

The ratio of minimum to maximum stress is the stress ratio, R, and is defined in (2.2).

$$R = \frac{\sigma_{\min}}{\sigma_{\max}} \tag{2.2}$$

If the cyclic loading has equal parts in compression and tension, i.e. $\sigma_{\max} = -\sigma_{\min}$, the stress ratio is -1 and is refered to as *fully reversed cyclic loading*. A stress ratio equal to 0 implies that $\sigma_{\min} = 0$, hence the component is unloaded during bottom part of the loading cycle. Static loading is obtained if $R = 1$, i.e $\sigma_{\max} = \sigma_{\min}$.

The stress ratio affects fatigue performance where an increased stress ratio extends the fatigue life. If the stress range is constant an increase in stress ratio lowers applied mean stress and on the other hand, if mean stress is constant an increase in stress ratio decreases applied stress range. From this reasoning, comprehending the direct stress ratio effects are not difficult. The stress ratio is usually kept constant and a common choice in tests are 0.2 [2c] and will also be adapted in the experiments herein.

Stress ratio might also influence the fatigue life of a component in the stage of fatigue crack growth, i.e. propagation and it has been shown that fatigue crack growth rate increases with a high stress ratio [13]. It is well established that the degree of crack closure increases with a decrease in stress ratio, however the effect of crack closure is debated regarding if the effect is present during early stages of crack initiation or merely develops during crack propagation [14]. Consequently, stress ratio may, in addition to above, also have microstructural effects which influence the fatigue life. Regardless, it is well established that differences in stress ratio alters fatigue test results.

The stress ratio for a real bridge in service is a function of the ratio of dead to live load and Tilly [1] reports in an overview article from 1979 that a common service stress ratio for bridges is between 0.2 to 0.4. Few newer stress ratio suggestions for real bridges have been found in literature, however Yafei et al. [13], suggested in 2017, that stress ratios in bridges are below 0.5.

2.1.3 Mean Stress

The middle value of the stress cycle is the mean stress, shown in (2.3).

$$\sigma_{\text{mean}} = \frac{1}{2}\left(\sigma_{\max} + \sigma_{\min}\right) \tag{2.3}$$

If the mean stress is increased, the allowable stress range decreases for a given number of cycles to failure [1]. Mean stress effects are many times overlooked, for instance in design codes such as *Eurocode 2* [3] and *fib Model Code 2010* [5]. The reason for this is somewhat unclear though a feasible assessment could be the stress concentrations at rib-bar locations and residual stresses from welding and manufacturing process yielding minor mean stress effect. Fatigue crack will always initiate at a material zone where stress concentration is large. Since rebars have both geometric discontinuities as well as residual stresses, mean stress effects might be less important when compared to a component where these properties are minimized.

2.1.4 Discontinuities and Temperature

As mentioned in Section 2.1.3, discontinuities have a major influence on fatigue life. Overall geometrical changes has the same effect in cyclic loading as in static, i.e. stress concentrations become an evident effect at these sites. For a rebar

the zones between bar and ribbing pattern are zones of stress concentrations as well as any welded surfaces.

Temperature has a clear effect on fatigue properties in two ways. Firstly, a change in temperature might alter material microstructure, hence the fatigue performance is not as intended. Secondly, thermal fatigue is also an issue where fluctuating temperature causes alternating stresses in the material similar to stress ranges. Temperature effects become more apparent at large alterations and are assumed negligible from now on.

2.1.5 Connection Between Stress Range, Stress Ratio and Mean Stress

A delicate problem becomes evident when stress range, stress ratio and mean stress are studied in more detail. When it comes to experimental procedure it should be desirable to only alter one parameter in order to isolate its effect on results. However this is not possible in the case of fatigue testing. Given that stress range effect is tested, stress ratio and mean stress should be held constant yet if the stress ratio is constant, that implies alteration in mean stress. And vice verse, if a change in stress range is performed with a constant mean stress, this consequently changes the stress ratio. This is not surprising since all parameters are functions of maximum and minimum stress, c.f. (2.1), (2.2) and (2.3).

2.2 Fatigue Approaches

Perhaps the most classical approach in fatigue design is the *total fatigue life*, N_f, an approach in which the number of cyclic loadings for a given stress range (or strain range) to develop catastrophic failure are counted and plotted in a S-N curve (*also* Wöhler curve). S (*or* $\Delta\sigma$) is the stress range and N_f are the number of load cycles to catastrophic failure. Fatigue strength is the reverse situation, i.e. the stress range for which a structural component can endure given a specific number of loading cycles. Figure 2.2 presents design S-N curves from EC2 [3a] where reduction in fatigue life for weld affected rebars are obvious, which are further discussed in Section 2.5.3. From Figure 2.2 it appears that welded rebars have a fatigue strength which exceeds that of unaffected rebars at high stress ranges, approximately $\Delta\sigma \geq 225$ MPa. This is however from mathematical aspects and not the case in reality. When design is performed, it is the S-N curve for unaffected rebars at these high stress ranges which apply since it is more conservative.

Another approach is the *defect tolerant approach* which also is known as *fracture mechanics* where by numerical simulation it is possible to asses a components crack propagation given a starting flaw. Both the *total fatigue life* and the *defect tolerant approach* are discussed more closely in Section 2.2.1 and Section 2.2.2.

A distinction is necessary to introduce between low-cycle fatigue (LCF) and high cycle fatigue (HCF). Low cycle fatigue characterizes of high maximum stresses where macro plasticity stresses occur in different extent in the steel during a loading cycle yielding low fatigue life. Load cycle stress levels entirely in the elastic material domain provide longer fatigue life and are defined as high-cycle fatigue [15p]. A precise and general limit for the number of cycles

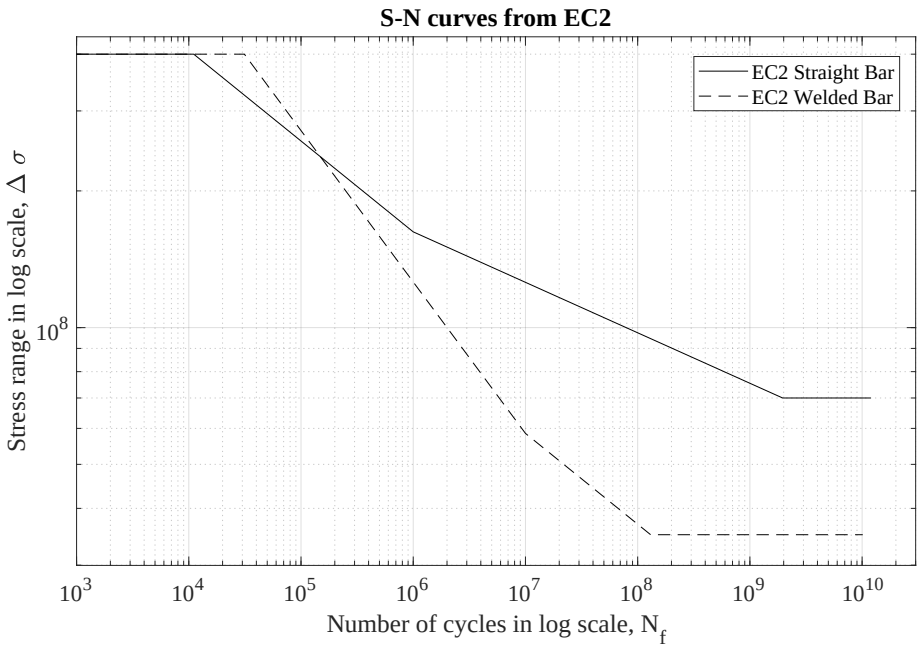

Figure 2.2: S-N curves from EC2 for straight unaffected rebars as well as weld affected rebars [3a]. The upper horizontal limit is the yield strength.

between LCF anf HCF is difficult to ascertain and is related to material properties and stress concentrations, however a reasonable assessment is somewhere in the region of $N_f = 10^4$ cycles [16].

Current fatigue evaluation approaches all rely on empirical data based on experiments and fracture mechanics, thus no analytical model exist. The physics of material fatigue are not yet fully understood, still an overview of current research position are reviewed.

2.2.1 Stress - Life Approach

The original *Wöhler approach*, i.e. where the total life, N_f, in terms of cycles to catastrophic failure, is connected to a specific loading level, such as stress range, $\Delta\sigma$, or stress amplitude, σ_a. Below a certain *cut-off limit* or *endurance limit* in the loading level, a detail is assumed to endure an infinite number of cycles and in Figure 2.2 the endurance limit can be seen where S-N curves turn horizontal. If this limit exists in reality can be questioned, however S-N curves show an obvious decrease in curve inclination when the number of cycles grow large from a decreased stress range. Typically, inclination changes somewhere in the range between 10^6 and 10^7 loading cycles, depending on material and starting conditions for a component or specimen [15q]. For smooth specimens, the *total fatigue life* approach, represents in many ways design against crack initiation since smooth specimens show a major part of their total fatigue life in crack initiation phase [15c]. In contrast, rebars are far from smooth and stress concentration as well as other surface defects are always present, especially at construction sites.

In 1910, Basquin suggested that fatigue life could be described by a power law function, presented in (2.4), where N_f is the fatigue life in number of stress cycles, $\Delta\sigma$ is the applied constant stress range and k and C are material constants.

$$N_f = C\Delta\sigma^{-k} \tag{2.4}$$

By using logarithms (2.4) becomes linear, as shown in (2.5).

$$\log N_f = \log C - k \log \Delta\sigma \tag{2.5}$$

From (2.5) it is evident that the material constant k describes curve inclination in log scale and C is the ordinate crossing.

The aforementioned description of a stress-life approach for determining fatigue life assumes a constant stress range throughout the entire life of the structure. In reality, this is not the case, where fatigue prone structures are subjected to varying stress range, mean stress and stress ratio. A more reality descriptive approach is available by the *Palmgren-Miner cumulative damage rule*, see (2.6), in which it is assumed that each load cycle, with a specific stress range, induces damage to the material. The damage from each cycle is added together and when the cumulative sum reaches a critical value (often 1) the detail fails. If n_i is the number of load cycles corresponding to a constant stress range, m is the total number of blocks of different stress ranges and $N_{f,i}$ is the fatigue life corresponding to the same stress range, (2.6) provides an estimation of the remaining fatigue life.

$$\sum_{i=1}^{m} \frac{n_i}{N_{f,i}} \leq 1 \tag{2.6}$$

The Palmgren-Miner rule should be used with caution. It can provide both accurate and inaccurate results, since the rule is load history sensitive, i.e. the outcome can differ vastly depending on assumptions of loading sequences. Furthermore it is a linear damage rule which overestimates damage from stress concentration such as notches and residual stresses. It is established that notches and residual stress concentration locations have the ability to non-linear stress redistribution when plasticity occurs. Finally, effect of crack closure is not considered, an effect more prominent the more minimum tensile stress is decreased and in particular during compressive loading [15s]. In summary, the Palmgren-Miner rule can be very helpful used under plausible conditions and assumptions.

2.2.2 Fracture Mechanics Approach

A different route can be chosen, if a *defect tolerant* approach is the basis, which is a fundamental assumption in *fracture mechanics*. The starting point is assuming the presence of flaws in all structural components. This premise is not hard to comprehend, however sizes and extent of flaws need to be determined, which in most cases are very qualitative and thus difficult to perform in an objective manner. Several techniques are available for examination of a specimen, yet none of which are perfect. Once initial flaws or crack sizes are settled, calculations determining the number of cycles to propagate the initial crack to a predetermined crack size or fracture, are performed [15b]. This can be

performed with satisfying result, given enough available experimental result for model calibration.

The overall idea, in fracture mechanics, is that by introducing a stress intensity factor, ΔK, the behaviour of crack growth can be assessed. Through numerical simulation, crack propagation can be modeled with finite element analysis [17g]. The well known *Paris law*, which still is most widely used, states that crack propagation rate is a power law function, as shown in (2.7).

$$\frac{da}{dN} = C\Delta K^m \tag{2.7}$$

where da/dN is crack propagation rate as crack growth, a, per cycle, N, ΔK is elastic stress intensity factor at crack tip and C and m are material constants which are functions of material microstructure, environment, temperature and stress ratio. As a consequence, it is not surprising that (2.7) only holds for constant stress ratio loading, as well as fixed environment and temperature [15u].

2.3 Material Microstructure

In order to describe the phenomenon of material fatigue behaviour properly, material microstructure content and texture are of great importance in all materials. Hereinafter, metal microstructure is the main focus which in literature is grouped under a material subdomain as *ductile solids* or *semi-ductile solids*. Generally a coarse delimitation between *ductile*, *semi-ductile* and *brittle* solids is necessary since differences in fatigue behaviour are known, however brittle materials are not discussed further.

Crystalline materials are composed of a distinguishing atomic arrangement which is important if material damage and fracture are studied and by extension fatigue damage. The crystalline microstruture as well as inevitable microstructural defects are discussed in forthcoming sections.

2.3.1 Crystal Types and Unit Cells

Metal microstructure is in essence crystals of various sizes which forms grains in the metal structure as a lattice. Crystals are arrangements of atoms in specific patterns which repeats itself in three dimensions [18a]. A crystal in the metal lattice can have an arbitrary rotation compared to other crystals in the lattice even though the atom arrangement remains the same. A distinction is made between single crystalline metals and polycrystalline metals where single crystalline metals are composed of only one chemical specific crystal structure. All other types are polycrystalline metals where different types of crystals are present in the metal microstructure. Polycrystalline metals are by far the most common metals since most engineering applications use alloys, which quite frequently show polycrystalline structure [15g].

When crystals form and grow, various manufacturing processes as well as chemical composition dictate which specific crystal structures are created. The smallest compound in a crystal is the unit cell which is a specific structuring of atoms. When a metal is manufactured, crystals grow from stacking of these unit cells face to face thus, unit cells are the building blocks in a crystal [18a].

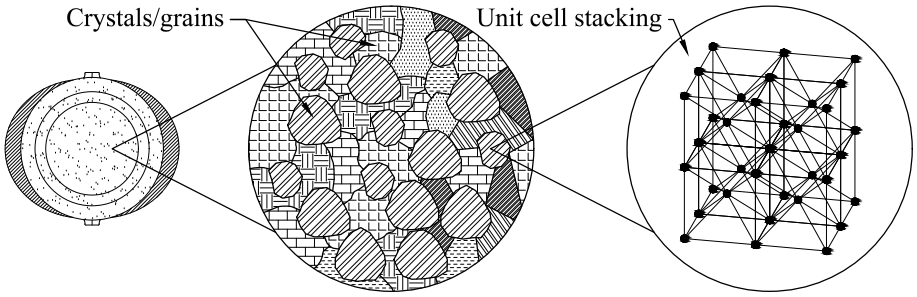

Figure 2.3: Rebar cross-section showing an arbitrary crystal structure as well as stacking of BCC unit cells within a crystal.

Figure 2.3 depicts how stacking of unit cells forms small crystals with varying size and orientation whereby the crystallographic lattice shapes the rebar steel. Several different unit cells exist and common crystal structures, relevant to metal microstructure, are face centered cubic (FCC) crystals, body centered cubic (BCC) crystals and body centered tetragonal (BCT) crystals. Differences in crystal structure result in varying general properties thus also fatigue characteristics. A FCC unit cell is shown in Figure 2.4 and is characterized by the face structure where six atoms, one at each cube face, are split at the faces between different adjacent unit cells. Each corner of a unit cell has one eighth atom thus shares this atom with seven other unit cells, see Figure 2.4a. The atom structuring over the cube faces is outlined in Figure 2.4b. A BCC unit cell still shares one eighth atom at the corners of the cell, yet one atom is at the center of the unit cells not shared with any other adjacent unit cells, which is presented in Figure 2.5a. Figure 2.5b highlights the atom structuring and specifically the centering of one atom to the cube body. FCC and BCC unit cell both are of cubic form, however different geometries are possible. If, for instance, the height of a unit cell increases, yet the same atom structure, a tetragonal geometry appears. A body centered tetragonal (BCT) structure is an example of this where the atoms are structured as in a BCC cell, however with a cell geometry of a cuboid. The only difference between BCC and BCT unit cells are thus the side lengths of the unit cell [18b].

2.3.2 Crystal and Structural Defects

An ideal crystal where stacking of unit cells are without flaws do not exist in real metal. On the contrary, all crystals contain defects which origin from either *point*, *line*, *surface* or *volume* imperfections. These defects are sources of disturbance to regularity of atoms and may significantly modify material characteristics which can be both positive and negative. The disturbance from defects introduce atom dislocations due to energy reasons. Dislocations are *line defects* and are of great concern in fatigue behaviour, however all defects influence fatigue properties [18c]. Dislocations are further discussed in Section 2.3.3.

In a perfect crystal all atoms are at specific and regular sites. As mentioned above, in a real atom structure *point defects* are present to some extent which may be *intrinsic defects*, i.e. positions where atoms are either left out as *va-*

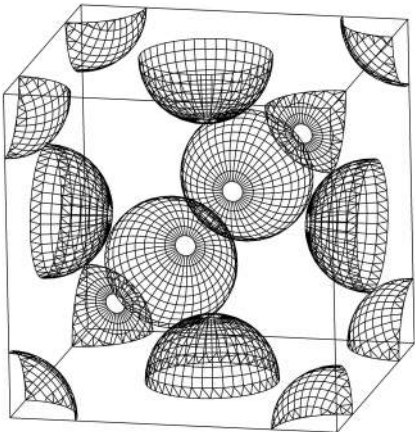

(a) Schematic view showing atom partitioning.

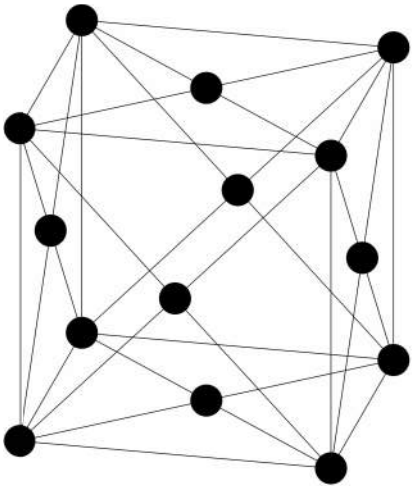

(b) Schematic view outlining atom structuring over cubic faces.

Figure 2.4: One unit cell of a face centered cubic (FCC) crystal. Inspired by [18m].

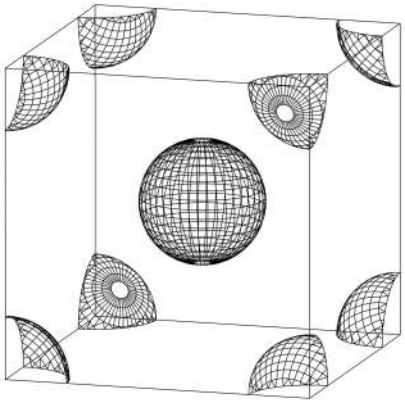

(a) Schematic view showing atom partitioning.

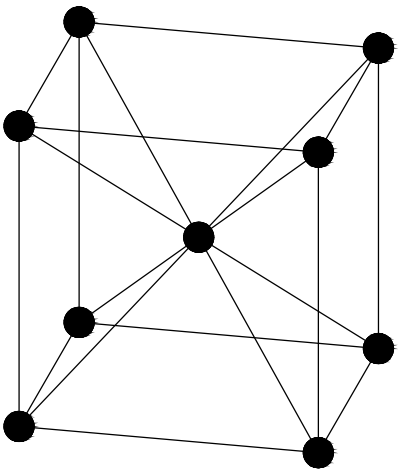

(b) Schematic view outlining atom structuring where an atom is centered to the cube body.

Figure 2.5: One unit cell of a body centered cubic (BCC) crystal. Inspired by [18l].

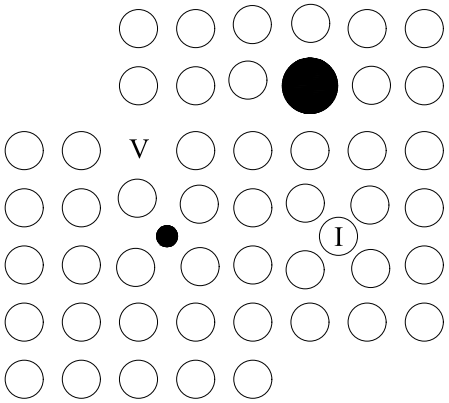

Figure 2.6: Schematic view of a metal plane showing point defects, impurities and geometry notches. V is for vacant atom position, I is for self-interstitial atom and black circles marks impurity atoms. Inspired by [18n].

cancies (V) or extra atoms are squeezed in as *self-interstitial* (I) atoms. Such positions are schematically shown in Figure 2.6 as "V" and "I". These intrinsic defects originate from energy entropy where a thermodynamically stable configuration generates imperfections, however vacancies or self-interstitial sites in atom arrangement, can also arise from plastic deformation or irradiation [18c]. Described point defects in atom structure are from atoms of the same base material, e.g. iron (Fe) in steel. *Impurities* are different atoms and are considered as extrinsic point defects. Impurities can have both positive and negative effect on material behaviour and are shown as black circles in Figure 2.6 [18c]. For instance, carbon (C) is added to some extent to Fe, in order to produce high strength steel but may also introduce dislocation to atom structure. Point defects interfere with the surrounding unit cells within the crystal yielding distortion effects to energy balances between atoms. The distortion may either increase or decrease the elastic strain energy within the crystal thus altering crystal loading performance [18j]. Point defects can introduce continuous atom dislocations over planes in the material which are line and surface imperfections, see Section 2.3.3. Volume imperfections can be of geometrical nature from atom dislocation originating from component shape.

Up until now, imperfections have been discussed as to *intra* crystal defects. A real crystalline material does not consist of one big crystal with flaws, furthermore crystals are not large compared to material macro scale, as for instance a rebar. Each crystal can be seen as a grain in the metal matrix with varying size and complex form, see Figure 2.3. Together these grains form the construction material and grain sizes and boundaries are other important features of material performance. Grains have different crystallographic orientation in the metal matrix yielding a very complex atomic arrangement at grain boundaries [18c]. Grain boundaries are important since these zones also present dislocation of atoms and a feasible assessment is the possibility of grain boundary dislocations affecting surrounding crystals hence inducing further dislocation within adjacent crystals. Moreover, during crystallization, grains grow in all directions yielding that some grains grow at the expense of others, thus dislocations in grains

are introduced from pushing and squeezing between adjacent grains [18i]. There are evident differences between single- and polycrystalline metals when it comes to deformation and yielding. In polycrystalline material structures, grains are more prone to have different crystal orientation and size as well as the obvious disparity between unit cells, compared to a single crystal material. This feature presents differences in micro plasticity, where the resolved shear stress may vary in individual crystals causing grain yielding to occur grain by grain. Boundaries between grains are also known to act as locking mechanisms during micro plasticity which is one explanation of the material hardening often seen in stress-strain curves between macro elastic- and plastic regions. As mentioned above, dislocations can *pile-up* at grain boundaries from locking mechanisms between crystals, however shape changes of grains and dislocation pile-up can induce dislocations in adjacent grains. This implies that macro plasticity, the stress at which all grains yield, is strongly related to average grain size [18k].

2.3.3 Dislocations and Slip Systems

The importance of material microstructure was emphasized in Section 2.3.1 and 2.3.2. Discussed defects, imperfections and stacking faults of unit cells, all contribute to dislocation in the atomic structure which are irregularities in metal bonding [18d]. Such dislocation sites in the atom arrangement are zones of possible microstructural movement, especially during loading. An important concept to grasp is *resolved shear stress* which induces dislocation movement. Consider Figure 2.7: if a material is subjected to a force, F, this force can be resolved over a slip plane area, $A/\cos\alpha$, where dislocations are prominent, hence a resolved shear stress, τ_r, is acting over that area. Dislocation movement is atom planes gliding over each other on account of the resolved shear stress.

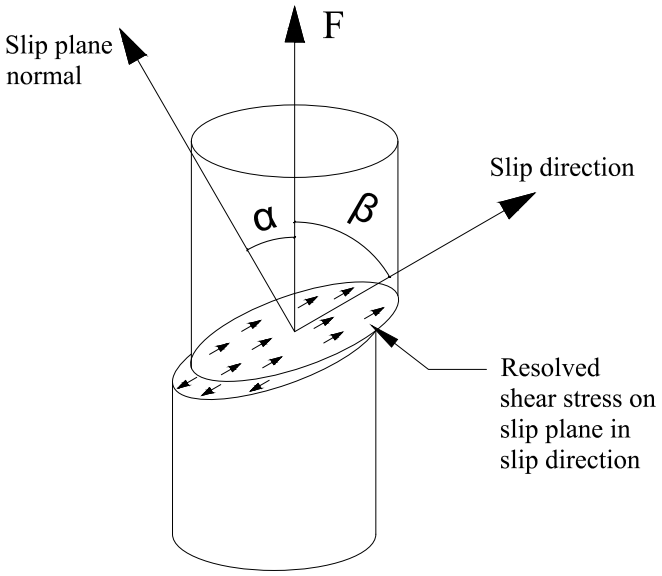

Figure 2.7: Definition of resolved shear stress. A force, F, acts in longitudinal direction which can be resolved as shear stress on a slip plane with a slip direction. Inspired by [18o].

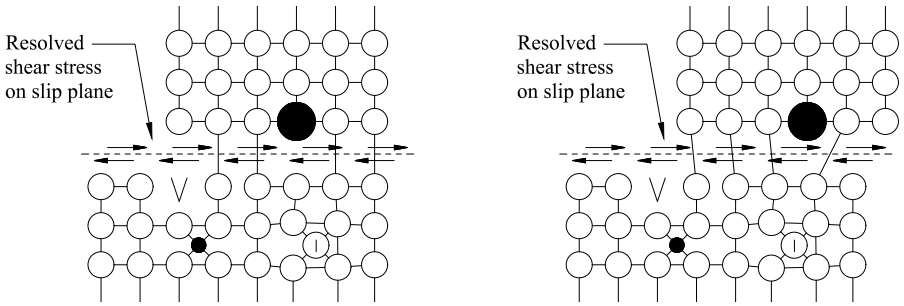

(a) Slip plane movement before atom translation.

(b) Slip plane movement after atom translation.

Figure 2.8: Slip plane movement induced by resolved shear stress where dislocations in atom structure are prominent. Inspired by [18p].

When several dislocations are involved in movement over a plane in the material, it results in a *slip plane* which is the first indication of plastic deformation. From the slip plane area along with the slip direction the resolved shear stress, τ_r, can be calculated according to (2.8) [15d, 18e].

$$\tau_r = \frac{F}{A} \cos\alpha \cos\beta \tag{2.8}$$

Figure 2.8 shows atom bonds switching when a slip plane is activated from resolved shear stress causing gliding of atom planes. The surrounding metal matrix remains undistorted during *slip* and further deformation occurs either on existing slip planes or by the formation of new slip planes. Generally, slip planes emerge where atoms are most widely spaced and slip directions are often shown in the direction where atoms are most closely spaced. This implies that atom structuring, as to unit cells and dislocations, are governing of slip plane locations and movement direction of slip planes in the material. A *slip system* is a slip plane with an associated slip direction and the number of possible slip systems are limited for a crystal structure [18e]. It should be noted that dislocations and slip systems in general are irregular and figures herein are simplifications of real slip systems [18f]. In general, by increasing unit cell complexity as well as introducing other atoms, e.g. for enhanced function of an alloy, slip systems rapidly become complex [18g]. As will be discussed in forthcoming Section 2.5, BCC and BCT crystals are of special interest due to rebar microstructure where a major part of the steel consists of either of these crystallographic structures. In a BCC crystal, slip directions most frequently are directions were atoms are most closely packed and slip planes are often located to planes of maximum resolved shear stress. In general, any plane with dislocations and resolved shear stress is a potential slip plane, however for a BCC crystal at room temperature, slip planes tend to show at maximum resolved shear stress. Slip systems are anisotropic when it comes to applied stress in order to induce slip, i.e. a stress level needed to dislocate atoms in one slip direction is not necessarily the same level to dislocate in opposite direction, given the same slip plane [18h].

2.4 Fatigue of Metals

Fatigue in material science is, by definition, cyclic loading causing damage and subsequently failure to a detail or structure. The cyclic loading can be, relative to the ultimate static loading, small for a failure to occur. The straining of the material microstructure, given enough loading cycles, entails microstructural damage as dislocation movement and slip systems where cracks can initiate. Furthermore, initiated cracks later propagate which leads to large visible macro cracks and total collapse. The fatigue life of a structural component may with the above in mind be divided into different stages, where the most general and wide description is presented below [15b].

1. Microstructural changes cause permanent damage.
2. Microscopic crack initiation.
3. Microscopic crack growth and coalescence forms more dominant cracks, hence a demarcation between crack initiation and propagation.
4. Propagation phase and dominant macrocrack accrue.
5. Failure, often as complete fracture.

The surrounding conditions and microstructural contexture strongly influences the rate between these phases and boundaries are seldom obvious. In practical engineering applications such as design of structures or experiments the above five stages are often simplified to three stages as *crack initiation*, *crack propagation* and *catastrophic failure* phases. These three demarcations are more visible when a fracture surface is studied without high-end equipment thus more relevant to engineering applications. A fatigue fracture surface is typically characterized by these three stages when studied by eye inspection. Cracking initiates at some site where stress concentrations are large together with flaws in the material surface. The crack starts to propagate which develops a smooth surface on macro scale and a somewhat jagged or wavy surface on micro scale from each load cycle known as *striations*. The cracking causes stress to rapidly increase over the remaining cross-sectional area by which a sudden and brittle fracture occurs when a critical stress is reached. This marks the third part of the surface fracture area and is rough and grainy from brittle failure [11a]. Figure 2.9 shows fatigue stages from a schematic view, where striations are displayed in zone two, together with a picture from specimen one, where the smoothness of zone two is evident on macro scale.

2.4.1 Fatigue Deformation

The fatigue phenomena is not fully understood despite significant research progress during the past decades. The first reports and attempts to describe the fatigue phenomena in a physical manner dates back to the early 1900'ies where *active slip planes* were first reported in studies from cyclic loading. The electron microscope enabled substantial progress of microstructural material behaviour during cyclic straining. Pure single crystalline FCC metals have the most conclusive results when it comes to fatigue deformation mechanisms. On the other hand, polycrystalline metals are more complex and thus quantitative treatment

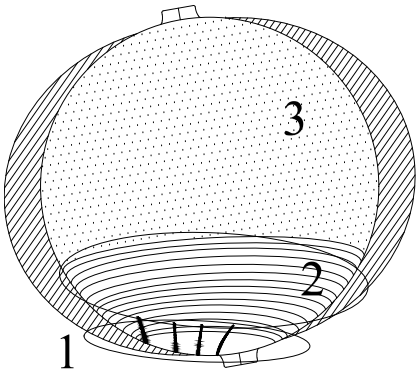

(a) Schematic view highlighting 1. perpendicular (to propagation direction) large cracks at initiation site, 2. propagation zone with striations and 3. fracture surface.

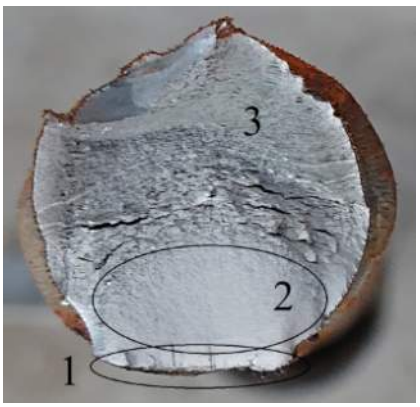

(b) Picture of fracture surface from specimen 1 from experiments where the differences between zone 2 and 3 is evident. Zone 2 show the smooth propagating phase in macro-scale and zone 3 display the sudden and brittle failure with a rough surface.

Figure 2.9: Schematic and pictorial view of a rebar cross-section showing fatigue stages as 1. crack initiation, 2. crack propagation and 3. brittle fracture.

is hard to obtain when viewed under microscope since several mechanisms might be active simultaneously [15a].

As listed and discussed in Section 2.4, microstructural changes causing damage to the material is obtained from fatigue deformation on micro material level. For a single crystalline metal, *active slip planes* can be identified during cyclic straining, which are planes where atom dislocation movement occur. As defined in Section 2.3.3 a force, F, acting in an uniaxial direction is resolved over a slip plane of the material whereby slip is initiated, see Figure 2.7. According to the *Schmid law* a crystalline solid flows plastically when a critical value of the resolved shear stress, τ_c, acting on the slip plane and in the slip direction is reached. Accordingly, if this critical stress, τ_c, is reached, micro plasticity by shearing to a slip plane implies *irreversible slip* in the material. In summary, if the straining induces slip in the material the cyclic loading generates a "back an forth" motion to slip planes in the slip direction, i.e. *active slip planes*. For a polycrystalline metal dislocation movement occurs by the same principle, however since the material is composed of varying crystals as to orientation and unit cells, multiple slip systems can be activated simultaneously in different directions and on different planes generating complex microstructural behavior [15d].

During loading three stages of fatigue deformation on microstructural level can be distinguished as shown in Figure 2.10. First of all, it should be emphasized that a constant plastic resolved shear strain, $\gamma_{r,pl}$, results in resolved shear stress which in general is a non-linear relation. For every cyclic loop in the loading, given constant plastic straining the resolved stress changes slightly until a the stress strain relation is more or less constant. This is known as the *hysteresis loop* and when a stable configuration for the stress - strain relation is reached,

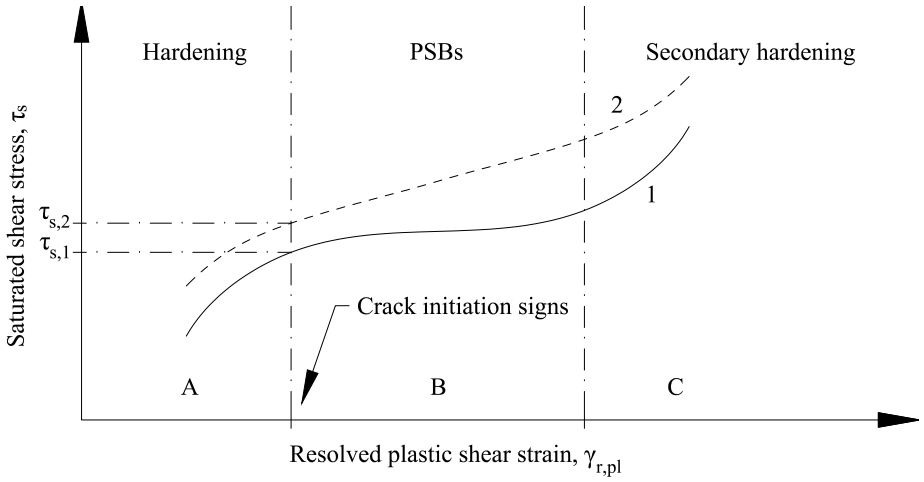

Figure 2.10: Saturation stress - strain curve, i.e. Resolved shear stress as a function of resolved plastic shear strain. Inspired by [15w].

saturated resolved shear stress, τ_s, has evolved. For every resolved plastic shear strain there is hence a corresponding saturated resolved shear stress [15e].

Cyclic work hardening occurs in region A, see Figure 2.10, which is activation of primary slip planes as dislocations, most prone to movement, are set in motion. Continued cycling accumulates dislocations and networks of dislocations arise which are referred to as *veins*, *bundles* or *loop patches*. The material hardening causes resolved shear stresses to increase over the slip planes nevertheless, when strains reach a certain value the material hardening decreases. For a single crystalline material with uniform crystal orientation a clear plateau is noticed after initial hardening, see curve 1 in Figure 2.10 and stress saturation, $\tau_{s,1}$, is reached. This plateau marks the beginning of region B and the formation of *persistent slip bands* (PSBs). Persistent slip bands are a very typical feature of initial stress saturation and are a banded structure of slip planes. In region B, the saturated stress increases much less for an increase in plastic strain which is typical for PSB formation in single crystals. For polycrystalline metals, slip planes can be oriented in multiple directions independent of each other and are thus referred to as multiple slip. From multiple slip, polycrystalline materials exhibit varying saturated stress strain curves and a generalized curve is nonexisting. For instance the clear plateau during PSB formation is not a necessity in general as curve 2 shows in Figure 2.10 where cyclic hardening continues in region B [15e].

PSBs are thus slip systems activated from resolved shear stress forming a banded structure on the material surface. It has been shown that fatigue crack initiation can be discovered along PSBs where slip is intense, furthermore these PSBs keep reappearing at the same locations of specimens during cyclic loading even after PSBs have been removed and cycling resumed. Studies have shown that PSBs are softer than the surrounding metal matrix implying that the initial material deformation, i.e. before cyclic saturation, is entirely carried by the PSBs. There seems to be some connection between the formation of PSBs and the stress-strain relation where a clear plateau is noticed during PSB formation,

however, in present day, no absolute explanation can be provided as to this phenomenon [11a, 15e]. The PSBs are composed by large number of slip planes and the damage mechanisms governing this are difficult to model since very local parameters such as grain size, grain boundaries, local stress concentrations and specific and local crystalline structure determine these mechanisms [11a].

As mentioned above, single crystalline metals oriented for single slip show two main features; the plateau region after cyclic saturation and the formation of PSBs with its prominent wall structure. When the subject is expanded to polycrystalline metals, which have a more complex microstructure, these features are not as obvious. Polycrystalline metals show different slip orientations as well as multiple slip systems when cyclic deformation occurs. Plateau region and PSBs are sometimes less pronounced and sometimes not present at all. A possibility might be that crystallographic direction as well as crystal type in relation to applied load influence the plateau region and its supervention. A polycrystalline metal would by this idea have varying fatigue properties since several different crystal structures are present, hence the microstructural changes from cyclic deformation are varying and unclear in polycrystals [15j]. In summary, during cyclic loading on metal prone to multiple slip systems, the clear fatigue damage characteristics for single slip systems is still present. However, due to the multiple slip, these features disappear amongst each other from interference- and interlocking of slip systems.

In region C in Figure 2.10, secondary hardening starts and formation of a *labyrinth* and *cell* microstructure can occur. This is often pronounced in materials with multiple slip and cross slip between different slip systems. Suggestions have been made to the origin of region C. One explanation is that secondary slip systems emerge at interfaces between PSBs and metal matrix which spread in the PSBs along with additional material hardening. This secondary slip causes initially a labyrinth and eventually a cell-like structure in the PSBs from multiple and cross slip between primary and secondary slip systems [15f].

Interesting geometrical features can be shown for these labyrinth structures where the formation of walls are oriented in two directions and orthogonal to each other. One wall direction is always parallel two the loading direction, i.e. $[0, 0, 1]$ in a Cartesian coordinate system and the other wall structure is always directed in one of three possibilities, $[1, 0, 0]$, $[2, 1, 0]$ or $[1, 2, 0]$. The possibility of multiple slip and cross slip causes interacting locking mechanisms and a higher cyclic hardening rate is achieved compared to single slip [15g].

Commercial polycrystalline metal can significantly deviate from single crystalline metal in fatigue properties from the presence of impurities, precipitants and inclusions. The rise of PSBs can start from within the bulk of the material and travel through grains if the grain-PSB angle is small enough, hence grain sizes and PSB angles are of importance. Grain sizes are relevant for the initial period of cyclic hardening of the material where coarser grain texture show less hardening [15i].

It should also be noted that stress ratio may influence the appearance of stress-strain curves during cyclic loading. For fully reversed cyclic loading, rapid cyclic strain hardening is noticed. This effect is also present in tensile-tensile loading however not that apparent. One possible explanation is the rotation of the active slip planes. Consider Figure 2.7: if fully reversed loading is considered the slip plane angle β remains unchanged when loading is 0, i.e in the middle of the load cycle. If a tension-tension loading situation is considered, the β

angle has a permanent changes compared to the unloaded configuration hence the distortion of the slip planes are different for various stress ratios.

2.4.2 Fatigue Crack Initiation

Exactly when a crack is initiated is hard to define, since it generally is a question of the scale of observation. For instance, small dislocations in nano scale could be defined as crack initiation as well as a small crack visible to the naked eye.

A basic fatigue phenomena is that repeated cyclic straining leads to *active slip* on different slip planes in the material, as previously discussed in Section 2.4.1. A slip is a translation of atoms across a slip plane where a solid block moves with respect to the other in a slip direction. As previously mentioned, slip planes accumulate at certain positions in the steel crystal structures which appears as bands or lamellars of slip planes, as *persistent slip bands* (PSBs). Furthermore, these persistent slip bands facilitates irreversible shearing between bands and yields surface roughening where slip bands appear on the material surface. This surface roughening is manifested as hills and valleys in relation to the original surface area and are referred to as extrusions and intrusions, presented in Figure 2.11. The surface roughening from extrusions and intrusions function as micro notches and yields stress concentrations which induce further slip. If an extrusion grows large enough, a protrusion is formed containing several intrusions and extrusions [15k].

The interface between a PSB and the unaffected metal matrix is a discontinuity plane where abrupt gradients in density and dislocations are present. Such interfaces are sites in which cracks are initiated thus surface roughening is a strong indication of crack nucleation [15k, l]. As mentioned in Section 2.4.1, PSBs can grow from within the material, however these PSBs are often constrained by surrounding metal grains and are thus confined to individual grains. Surface roughening is consequently not possible for interior PSBs and is limited to near-surface PSBs. This implies that crack initiation is located at surface regions which underlines the established view of fatigue being a surface phenomenon. The importance of surface conditions have been demonstrated several times by electropolishing fatigued specimens after the appearance of protrusions whereby fatigue life is significantly enhanced [15m, n].

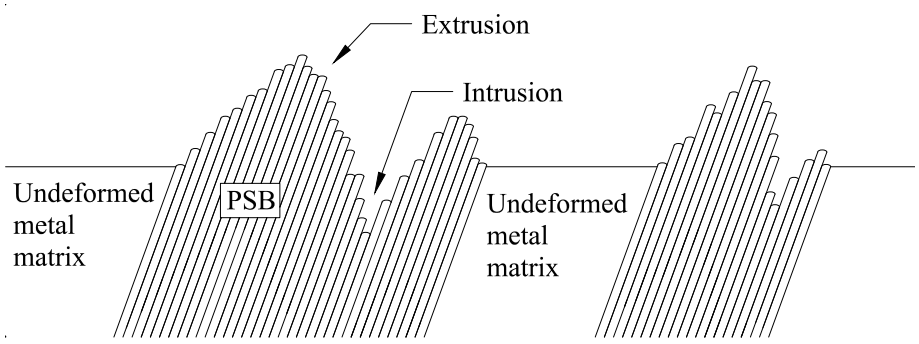

Figure 2.11: Intrusions and extrusions at PSBs zones where the typical occurrence of hills and valleys are shown. Inspired by [15x].

Commercial alloys are not pure or perfect, hence several defects and flaws exists whereby it is impossible to determine where a crack initiation is likely to occur. For reinforcing steel in particular rib structure, corrosion and welding all introduce notches and stress concentration in the metal matrix providing complex geometry as well as residual stresses [2c] all of which account for nucleation of persistent slip bands at these zones.

As discussed in Section 2.4, a distinction is necessary to make between *ductile*, *semi-ductile* and *brittle* material in order to describe crack initiation properly. For reinforcing steel of *quenched and self-tempered* (QST) type, there are mainly two different crystal structures, see Section 2.5.1. The rebar core of mainly ferrite (and some pearlite) show ductile behavior and is a BCC metal structure. The hard outer shell of martensite is of a BCT crystal structure and exhibits a semi-brittle material behaviour. This is not general material characteristics for BCC and BCT crystals, however it holds for ferrite and martensite respectively. A more brittle material is less prone to plastic flow and thus slip planes from dislocations is not the only factor that can initiate a crack. For a semi-brittle material bond rupture between atoms is also in play and with an increasing brittle material a shift is seen between dislocation mobility and atom bond rupture. In summary, for a highly ductile material the governing factor for crack initiation is dislocation planes and for a highly brittle material main factors are atom bond rupture. Thus, for a semi-brittle material both phenomena can cause crack initiation and to separate the one from the other is of course difficult in reality [15o]. A direct consequence is that cyclic deformation effects are harder to identify for more brittle materials.

2.4.3 Fatigue Crack Propagation

As mentioned in Section 2.4, the fatigue life can be divided into fatigue crack initiation, propagation and catastrophic failure. Once a crack initiation results in a small macro crack, this crack can propagate with increasing speed and complete fracture might develop rapidly. Crack propagation is influenced by *mean stress* and *stress ratio* as discussed in Section 2.1.2. In general, the rate of crack growth is related to crack length or depth into the material which in fracture mechanics are described by the increment da/dN, see Section 2.2.2. The crack propagation rate increases by the increase in crack length which results in the increase of growth rate with increasing number of load cycles [15u].

Fatigue crack growth is strongly influenced by microstructural texture which relate to slip characteristics at microstructural dimensions. Stress level affect propagation of course, where an increased stress level increases the material volume in which micro plasticity occur around crack tips. Crack propagation is intense local deformation at initiation zones or crack tips where macroscopic slip bands has emerged as discussed in Section 2.4.2 [15v].

The fatigue crack growth stage can itself be divided into additional subdivisions of *stage I* and *stage II*, shown in Figure 2.12. Stage I is obviously when macro cracking still is relatively small and identified as the crack being smaller than a few grain diameters. Furthermore, crack growth in stage I mainly occur through single shear in the direction of primary slip bands, creating a zigzag pattern when a crack finds a path along different slip systems in the material. When a crack grows, the plastic zone at crack tip intensifies due to an increase in stresses from decrease in cross-section area and plastic deformation in an in-

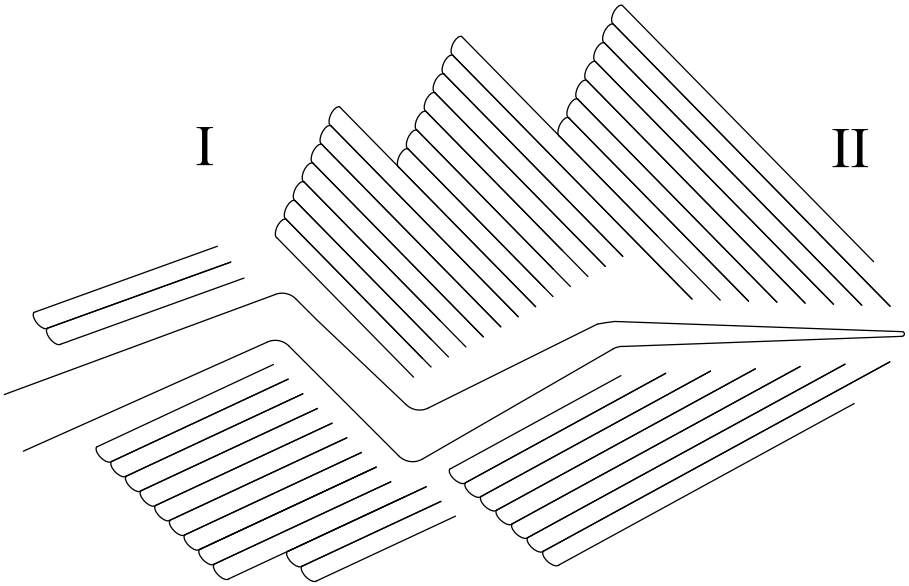

Figure 2.12: Schematic view of crack propagation stegs I and II. Initially crack growth follows the banded structure in stage I whereon crack cuts through bands in stage II. Inspired by [15y].

creasing amount of metal grains occur. When micro plasticity reaches a certain level, i.e the plastic zone becomes large enough, two slip systems can simultaneously be activated resulting in a duplex slip mechanism which is by definition stage II. This results in an end of the zigzagging of crack path and a planar crack growth pattern commences normal to the tensile loading which cuts through the slip bands. Figure 2.12 illustrates the differences between stage I and II where the crack at first finds a way parallel to slip bands whereon at a certain plastic loading level the crack evolve normal to loading direction and cuts through the slip bands. Stage I has thus a serrated profile while stage II exhibits a more smooth surface. During stage II a typical phenomena named *striations* appear on the crack surface as small ripples and the distance in between these striations correlate with crack growth during peak tension loading. Striations form in all ductile solids, however in steel they might be barely visible and infrequent from varying crystal structure [15v].

2.4.4 Static and Cyclic Loading - Differences

All the way back to the work of *Wöhler*, it has been obvious that cyclic loading differs from static. An absolute physical explanation is not available to this day, however differences in material damage have been documented [15h].

Initial material hardening can be seen during both cyclic and static loading. Material damage starts to differ at the formation of PSBs which is unique for cyclic deformation. Furthermore, the density of dislocations in persistent slip bands from cyclic loading is higher compared to monotonic slip bands produced under static loading. This is visualized in Figure 2.13 where the more compact banded structure is seen for cyclic loading in Figure 2.13a and less dense slip

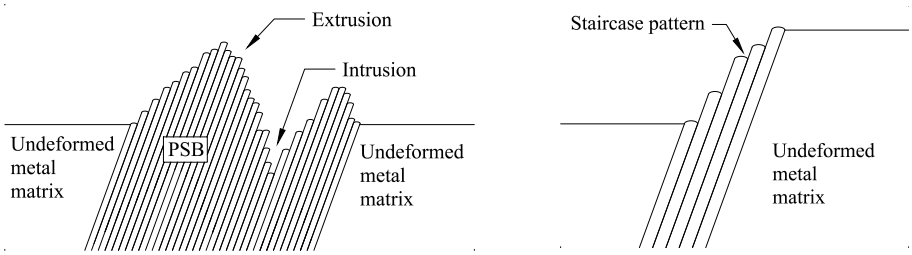

(a) Extrusions and intrusions from fatigue deformation.

(b) Staircase pattern from static straining.

Figure 2.13: Differences in material damage from cyclic and static loading respectively. Inspired by [15x].

bands for static loading in 2.13b [15h].

The clear plateau during cyclic loading, discussed in Section 2.4.1 and shown in Figure 2.10, is a typical feature of cyclic loading. As also mention, this plateau does not always appear due to alloying and complex material microstructure [15h]. Nevertheless, cyclic saturation in a material is an important feature, strongly related to material fatigue.

The *back and forth* motion of cyclic loading forms dislocation pile-up in crystals which may develop a high density of point defects a local spots in a crystal [15h]. This pile-up induce additional disturbances in energy balances as to atom structuring which intensify dislocation movement.

Finally, the specific pattern of surface roughening is a major difference between static and cyclic loading. The formation of extrusions and intrusions at material surface is typical to cyclic loading whereas static loading show a staircase pattern with clear steps, which is seen in Figure 2.13 [15h].

2.5 Reinforcing Steel

Structural concrete is almost exclusively reinforced with rebars. In forthcoming sections, rebar microstructure is discussed in relation to fatigue performance. Available literature from previous test result deemed relevant, is incorporated at appropriate paragraphs and the implications from welding are examined.

2.5.1 Microstructure of Reinforcing Steel

As mentioned in Section 2.4, steel microstructure has a strong influence on fatigue behaviour. Common reinforcing steel for concrete applications are manufactured by a *TEMPCORE* process eventuating in a *quenched and self-tempered* (QST) steel. In essence, the rebars are conventionally hot rolled, obtaining a temperature of approximately 1000° C resulting in austenite steel, which has a FCC crystal structure. Immediately after the hot rolling, the rebars are subjected to an instant high pressure water cooling thus the surface austenite undergoes a transition to martensite, a BCT crystal structure. The cooling process is performed only to retrieve a hard case of martensite, thus a hot core of austenite remains after the cooling. The rebars are now allowed to slowly cool down

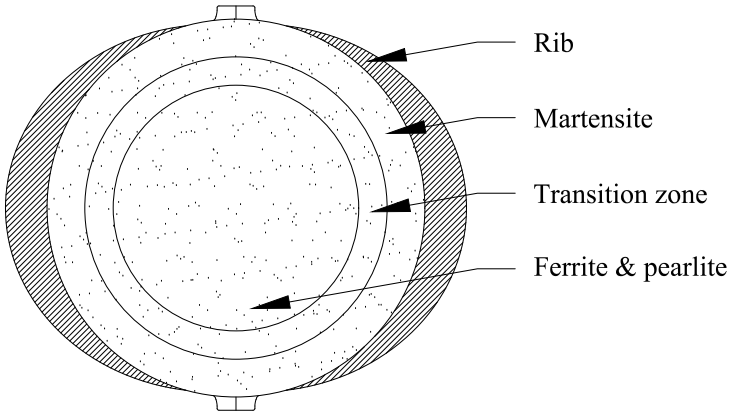

Figure 2.14: Schematic cross-section of quenched and self-tempered (QST) reinforcing steel where morphology is displayed.

to room temperature where the hard martensite is tempered by the hot core whereby some minor softening occurs. Finally the austenite core shifts to mainly ferrite, a BCC crystal structure. To an extent, the austenite core also shifts to cementite and the tempering of the martensite also results in some cementite precipitation. When ferrite and cementite is combined in a lamellar structure it is called pearlite, however, ferrite and cementite can also be combined in a non-lamellar structure which is known as bainite. To sum up, the resulting product is a ductile steel core of ferrite and pearlite and a hard outer case of martensite. In between these two steel crystal structures, a transition zone exists, composed of mainly bainite and ferrite. From the manufacturing process, both tensile and compressive residual stresses are known to develop, mainly on the surface and outer layers of the rebar cross-section [19]. Figure 2.14, shows a schematic cross-section of a QST rebar where the different zones of steel crystal structures are presented. The demarcations between zones are in a real rebar of course not that apparent however the general idea is shown.

Quenched and self-tempered (QST) rebars were investigated by Rocha et al. [20] as to residual stresses, imperfections along with a numerical analysis of rib spacing. Grain sizes increased with increased diameter of the rebar, however it was concluded that the grain size of QST rebars were smaller compared conventional to hot-rolled rebars. Samples from QST rebar cores showed ferrite grain sizes in the range of 7.9-11.2 μm and the area fraction of pearlite between 11-25%, still at the core. Tensile residual stresses near surface of the bars were no higher than 23% of their yield stress. Furthermore, it could be concluded that imperfections originating from the manufacturing process often were located near the ribs which give rise to stress concentrations. Numerical analysis also showed stress concentrations near rib and bar intersection, which could be lowered with decreased height of the rib along with an increase of radius between rib and bar, i.e a smoother transaction zone [20].

The microstructure of the material is of great importance to fatigue properties and resistance. Fatigue testing commonly experiences experimental scatter which for lower stress ranges can be significant. QST reinforcement bars with a core of ferrite-pearlite and a coat of martensite were examined by Rocha et

al. [21] as to a single short crack propagation in an attempt to understand and model experimental scatter. Martensitic microstructure contributed to a reduction in experimental scatter compared to ferrite-pearlite microstructure when stress ranges above fatigue limit were considered. Area fractions of ferrite-pearlite along with grain and phase boundaries were shown to affect the short crack growth rate thus increasing the scatter in fatigue crack initiation period. Since crack initiation mainly is a surface phenomenon an approximation could be provided postulating that half of the experimental scatter originates from specimen surface microstructure [21].

Yafei et al. [13] performed a study, where reinforcing steel was subjected to fatigue loading in an attempt to elucidate microstructural influence on crack patterns. The following microstructural analysis of crack paths revealed cracks running *through* the ferrite grains and *deflecting* once the crack encountered pearlite.

2.5.2 Fatigue Characteristics of Reinforcing Steel

Many studies are conducted on unaffected reinforcement bars which are summarized in for example [1, 2, 22]. Very seldom structural failure of reinforced concrete is due to fatigue damage in the concrete material. When concrete deforms, it cracks, thus the stresses are thereafter mainly carried by the reinforcement bars which also are more prone to fatigue failure compared to the concrete material [11g].

Fatigue in concrete structures is difficult to detect. The concrete itself shows few signs of fatigue symptoms and it is hard to distinguish causes between different cracks. The reinforcing steel is embedded in concrete making it hard to examine at all. Nevertheless, catastrophic failure of structures are rare and seldom linked to an isolated mechanism. Failures due to only fatigue have not been reported, however fatigue of concrete and rebars accelerates crack opening, crack width magnitude and by extension second- and third order stresses as well as corrosion of rebars. It should also be added that rebars can fail from fatigue without any outwards sign except concrete cracking where it is difficult to determine exact origin to a crack in the concrete. From the uncertainty of the loading and assumptions, calculations of stress ranges are difficult and design stress ranges are most likely to be high when compared to real stresses [1].

Since fatigue crack initiation of rebars tends to originate from surface conditions, these conditions may determine fatigue properties of reinforcement bars. Hot-rolled and cold-worked (HR-CW) rebars as well as quenched and self-tempered (QST) rebars were examined by Rocha et al. [23] with a *Navarro and De Los Rios model* trying to elucidate main characteristics influencing the fatigue behaviour of rebars as to crack initiation, including short crack growth and propagation. The model captured the scatter when compared to experimental result implying crack initiation phase is a major part of the fatigue life. The initiation phase is a stochastic process including the growth of microstructural short cracks. By simulations it could be concluded that 80% and 60% of the fatigue life for QST and HR-CW rebars respectively was linked to crack initiation phase. Furthermore, short cracks are allowed to grow to 10 times the grain size (~ 0.2 mm) before macro crack propagation phase starts. Finally, surface microstructure was deemed influencing the scatter in fatigue life by 50%.

Stress concentrations in the vicinity of the ribs on the rebar surface often

induce fatigue cracking as discussed above. Rib spacing is vital in order to reduce these stress concentrations as shown by Majumdar et al. [24] where rib spacing was studied while maintaining bond strength of the reinforcement-concrete interaction. Laboratory testing along with FE-modeling revealed that most of the fatigue failure initiated at the root of the ribs. It was concluded that rib spacing could be increased in some extent without affecting bond strength.

QST reinforcement bars were tested by Rocha et al. [25] and 80% of the 21 rebars survived more than 30 million cycles at stress levels near 50% of the yield limit. Fatigue cracks were hard to detect unless fracture was close in time. Finally it could be concluded that fatigue cracks initiated at surface imperfections located near the ribs.

Apostolopoulos and Rodopoulos [26] studied low-cycle fatigue of QST rebars, where focus was seismic application. However *as received bars* were used which entails the fact of small corrosion on rebar surface. The rebar surfaces were examined and it could be shown that these contained evident porosity, perhaps from trapped oxygen. Residues from copper (Cu) was also present at pores.

As previously mentioned a vast amount of reasearch exists on rebars in general. The perception on the field is however that many studies are somewhat outdated since the introduction of quenched and self-tempered (QST) steel. Overviews on rebar fatigue are dated back to the 1980'ies, see for example Tilly [1] and Bulletin 188 [2]. Of course they are still indeed relevant, however steel from this time shows differences to modern rebar steel when it comes to fatigue performance, as for instance QST steel. It has been pointed out by Tilly [1] that there is very little improvement of fatigue strength using steel with higher yield limit than 420 MPa. High strength steels might thus be questionable for structures having very high live loading causing cyclic straining if fatigue is limiting in design. Zheng and Abel [19], compared fatigue performance of QST rebars to other types of reinforcing steel where result points to a higher fatigue resistance of QST rebars. The result indicate that existing models fail to predict fatigue life of QST rebars and it is suggested that metallurgical microstructure and residual stresses from this specific manufacturing process is a contributing factor to the enhanced fatigue properties. The fatigue cracks were initiated from transverse rib roots in the martensitic layer. Zheng and Abel also state that fatigue properties in QST steel mainly are a function of the hardened tempered martensitic layer containing compressive residual stresses, claiming that fatigue performance is not significant to the core material of ferrite-pearlite.

2.5.3 Welded Reinforcement Bars

Welds tend to induce weakness to the structure because of regions of stress concentrations and poor material properties which vary through the weld and ambient heat affected zone. This is a major problem in industrial assessments where the difficulty lies in defining the weld geometry with sufficient accuracy along with required simplicity for design. Finite element analysis (FEA) can be used to model welds but a detailed analysis is required which results in impractical design situations where the number of welded components are countless [27].

Some case studies have been performed for concrete structures where fatigue issues were detected on in service structures and a general conclusion is that welding should be avoided for reinforcing steel [2a, b].

For reinforcing steel, the dominating parameters are *stress range*, *number of stress cycles*, and *discontinuities*, c.f. Section 2.1. Due to stress concentrations always present from manufacturing such as ribs and residual stresses from, e.g. quenching, it is assumed that *mean stress* is negligible [11b]. If a rebar furthermore is subjected to welding, this underlines above conclusion since the welding process introduces high residual stresses.

Welding of all types show very high vulnerability to fatigue damage and failure, thus the large reduction in fatigue strength in EC2 [3c] considering weld affected reinforcement bars are understandable [11h]. The considered welding in experiments herein is that of less impact on the reinforcement bar in question. The welds in question can be considered as non load-carrying where their only purpose is to keep the reinforcement in place during the concreting. The weld should be as small as possible, affecting the longitudinal bar as little as possible while still being able to maintain purpose. This is where industrial robots come in play since their ability to maintain a high level of weld quality is constant during production, i.e. there is not an lowering of weld quality from human factors such as long working hours or tiresome weather.

Tong et. al. [28] performed a study, examining the fatigue behaviour of reinforced concrete beams under bending loading. The concrete beams were reinforced with reinforcing bars as well as an H-steel beam. Main focus were fatigue behavior of the H-steel beam where fatigue fracture occurred in the welded areas of the steel beam. The H-steel beams were constructed of a welding procedure where flanges and web were welded together, hence it could be further substantiated that welds are weak spots regarding fatigue issues.

In order to simulate very local corrosion, rebars were tested in fatigue after artificially introducing notches at their mid span by light rasping of the material. An increased notch depth was shown to decrease the fatigue life [29]. A possibility might exist, that by introducing welds on rebars, the effect on fatigue life could be comparable to defects as local corrosion or notch effect, hence unaffected rebar cross-section area might show an important factor for fatigue life of a specimen.

An American study have performed tests similar to tests herein where fatigue life of rebars subjected to welding of crossing rebars were performed. The testing aimed for design suggestions for welded-wire fabric (WWF) in the U.S. hence the American standard was governing. Stress range and mean stress were varied resulting in a performance loss from approximately 165 MPa (24 Ksi) to approximately 110 MPa (16 Ksi) when weld affected rebars were compared to unaffected rebars. It should be mentioned that these stresses are not directly comparable to stress ranges as defined in (2.1) since American definitions of fatigue stresses were applied which involves both stress range and minimum stresses [30].

Welded-Wire-Fabric (WWF) is used in great extent in housing and other non fatigue prone structures since prefabrication simplifies production implementation. Ayyub et al. [31] performed fatigue testing on a number of different types of WWF, including with and without welded intersections, in order to evaluate the ability to used WWF in bridge construction. The result indicated that WWF meets the fatigue requirements for bridge decks. The stress range was varied and a constant minimum stress was applied to the specimens, thus maximum stress was altered, modifying the stress ranges. The experimental arrangement was similar to the testing herein, however different bar sizes were

used for different types of WWF making comparisons more difficult. It was concluded that the fatigue life of a welded specimen is lower compared to a specimen without a weld which appears as a parallel shift in a S-N curve. Accordingly the fatigue life was shorter for WWF and all crack initiations were located in the vicinity or in the welds. However all tested specimens had a fatigue life in excess, when compared to the American design standard, *(AASHTO)*, specifications for bridges. Furthermore, the electrical welding process itself was important since crack initiation appeared in some cases where pressure was applied, implying the importance of the skilled workers welding proficiency.

Butt-welded- as well as cruciform rebar specimens were tested in low-cycle fatigue attempting to simulate seismic loading. Results imply that butt-welding should be avoided near plastic hinges, however properly performed spot weld between stirrups and longitudinal rebars might safely be applied [32]. It remains to be seen whether the same effect can be shown for high-cycle fatigue, i.e. sufficiently unaffected longitudinal rebars providing prominent fatigue life results.

2.5.4 Welded and Fatigued Steel

Few studies of weld affected rebars exist similar to the testing herein and considered papers are reviewed in Section 2.5.3. Fatigue research of steel in general is more extensive and some fatigue studies on steel *cruciform* or T specimens might be relevant. A T or cruciform specimen is more or less self explanatory where two steel bars are welded together, forming a T or a cross. The welding is most often in plane hence two butt-welds are performed for a cruciform specimen and one for a T specimen. The construction steel is generally more ductile compared to rebars and has a lower strength, however similarities in experimental set-up exists and some relevant conclusions might be transferable to rebars.

Steel plate specimens, subjected to welding by a transverse cruciform joint were tested in fatigue in axial direction, i.e. the welds were non load-carrying. Specimens of thickness 20 mm and different widths all failed from fatigue cracks in the weld toe [33]. The main focus was evaluation of tensile residual stress magnitude, since small-scale specimen testing might have lower residual stresses when compared to larger structures with extensive welding.

Similar to above description, cruciform specimens with non load-carrying welds were tested in axial fatigue. Test results were compared to Eurocode 3 [34], concluding a good fit to the specified S-N curve [35].

Non load-carrying T fillet welded joints, i.e. two steel plates welded together perpendicular, were tested in three point bending fatigue. Gaping spaces between the two welded plates were investigated and it could be concluded that a gap showed higher fatigue performance compared to specimens where the welding was all out, i.e. there where no gap left between the two welded plates. Furthermore, test result of CO_2 welded specimens, were compared to fatigue class design (FAT) categories, showing higher fatigue performance [36].

T- and X-joints were tested in axial tensile and bending fatigue by Ahola et al. [37], evaluating fatigue differences between asymmetric and symmetric welded joints. The joints were constructed of steel plates as transverse non-load-carrying welded attachments and it could be concluded that T-joints had a higher fatigue resistance than X-joints. The X-joint increased the notch effect

at the weld toe, thus the decrease in fatigue life was expected. Furthermore, results presented higher fatigue performance in bending compared to axial tensile fatigue. Finite element analysis were also performed where the outcome supports the experimental result.

Weld geometry is shown to influence fatigue performance, where parallels can be drawn to rib geometry, i.e. geometry of imperfections are relevant to fatigue performance. Test result presented higher fatigue performance than design curves and it was observed that an increase in weld flank angle as well as weld toe radius increased fatigue performance of specimens [38].

2.5.5 Test Methods

There are two principally different ways of testing fatigue of reinforcing steel. Either an entire reinforced concrete component (usually a beam) of interest is tested in bending fatigue, or unclad reinforcing steel is axially tested in air on an *as received* bar without any concrete present. Axial testing in air is considered to be conservative since typically a 20% lowering in fatigue life is in general seen. Specimen failure at the gripping areas, due to high local stresses, is a possibility which renders questionable result of that specific test. The increase in fatigue performance in bending tests could be explained by the fact that the highest stresses not necessarily are located at the vicinity of the worst defects of the rebar which is the case for an axial test where the stress more or less is constant through the length of the rebar. Advantages with axial air testing is mainly that frequency can be high, up to 150 Hz without frequency effect on the result. Bending tests on concrete beams are more relevant to service conditions however frequencies are limited to about 5 Hz in order to avoid local heating due to friction between rebar and concrete which significantly prolong testing time. It can also be shown that fatigue test results, considering crack initiation sites, differ somewhat when axial and bending tests are performed and compared. For axial tests in air crack initiation is often located at surface defects while bending tests more often show crack initiation in the vicinity of the ribs. Another difficulty related to bending testing of a complete concrete beam is the calculation of stresses where an assumption is necessary for the load-carrying contribution of concrete as well as accuracy of reinforcement placing. Axial tests in air are easily calculated by a nominal approach with fair precision [1, 2d]. Welding in reinforcement produces higher reductions in fatigue strength when comparison is made between axial tests in air and bending tests of reinforced concrete [1]. This is hence on the safe side and safe for use in design purposes provided that corrosion is unlikely to occur.

2.5.6 Surface Attribute Effects

As discussed in Section 2.4.2, surface roughening with intrusions and extrusions is a potential crack initiation site. By extension, an initially rough surface is more prone to a crack initiation compared to a polished and smooth component. For a rebar, the surface is very rough originating from mild corrosion as well as ribs.

Surface treatment such as *welding* or *quenching* can introduce high residual stresses of yield stress magnitude which might produce high stress concentrations and local yielding of steel even for small succeeding loading. The tested

rebars in this study are both quenched and weld affected with spot welds at two locations, hence residual stresses are inevitably present. Residual stress fields alter applied mean stress and are in general favorable if compressive and unfavorable if tensile. Several methods exist, where the common objective is to produce compressive residual stresses in order to prolong service life of components [15t].

Studies of weld affected reinforcement bars are mainly focused on butt-welded bars thus the weld spans the entire rebar cross-section. The weld material itself is usually not an issue since it most often is stronger than the steel material. However, the zone between steel and weld matrix is fragile and crack prone. These tests are hence on load-carrying welds and parallels are hard to draw to non load-carrying welds, since the later case has a smaller heat affected zone as well as a partly unaffected cross-section.

2.5.7 Properties Influencing Fatigue Life of Rebars

Reinforcing steel has a pattern of ribs on the surface whose primary function is to ensure good bonding between concrete and rebar as well as obtaining pull out strength. The ribbing pattern is not chosen randomly since this ribbing highly influences fatigue life. A too small rib radius should be avoided and intersecting ribs are also unfavorable [24]. Since ribbing is needed, it is most important to ensure that other defects are minimized as much as possible. Identification markings and chipped mill roll are known causes of premature fatigue failure of rebars [2e].

An increase in bar diameter lowers fatigue performance, being a general size effect, not limited to reinforcement bars. This is explained by increased likelihood of surface defects since the surface area increases with increased bar diameter hence crack initiation is more feasible [1, 2f]. However, an increase in bar diameter also decreases the weld affected cross-section, since the relative heat affected zone is decreased compared to an increased cross-section area. It is hard to draw any conclusions from this, regarding fatigue of weld affected rebars, and experiments of different rebar sizes are necessary in order to determine how this two-sided effect relates to fatigue life of different sized rebars. Size affect also appears to be less pronounced in bending tests compared to axial tests in air where the same argumentation as above can be made of the decreased probability of a rebar defect coinciding with high stresses [1].

Bent bars reduce fatigue life and the reduction is a function of the bending radius and bar diameter. Performance losses are connected to bending induced stresses and stress concentrations at bending points during loading [2g].

Welding of rebars have been studied by several investigations, in order to determine the fatigue performance losses due to the welding. Some results indicate that the fatigue life can be as good as a straight unaffected rebar and other results show a fatigue reduction by 50%. Tests in bending produce better results than axial tests in air. A distinction is necessary between type of welds, e.g. butt-welding and tack-welding, as well as whether the weld itself is load-carrying. It is often unclear in literature what specific weld is addressed. Irrespective of this, welding of rebars in general reduces fatigue performance, thus in design standards welding is overall discouraged for fatigue prone structures.

There are comparatively few published data of fatigue tested welded rebars thus conservative design rules are not surprising. In general, axial tests in air on

welded rebars produce test results which are lower compared to bending tests. Since most tests have been performed in air this induces a conservative design standard which may unnecessary prevent the use of welding [1, 2h, i].

2.6 Fatigue in Eurocode 2

Fatigue damage mechanisms and a complete understanding of fatigue phenomena when it comes to reinforced concrete is still lacking. Present fatigue regulations for design are based on narrow knowledge when compared to other domains of structural concrete. A worst case scenario of fatigue action effect is considered in codes which often rely on experimental data with little scientific background [11d, 39a].

Design of fatigue prone structures are usually limited to infrastructural projects such as bridges or tunnels where live loading may result in prominent stress ranges. For standard building constructions fatigue issues are usually considered as negligible thus the design standard describes a calculation approach suitable for bridges. This approach is briefly presented in Section 2.6.1 and relevant parameters where an altering suggestion could be in question from experimental result are highlighted.

Selected parameters in the fatigue section in EC2 is discussed in Section 2.6.2 where background and reasoning to choices are presented.

2.6.1 Fatigue Design According to Eurocode 2

Fatigue design for bridges in EC2 [4a, b] separates concrete and reinforcing steel. For rebars an equivalent stress range is determined as shown in (2.9) where adequate resistance is assumed if the condition is met. γ factors are partial coefficients and $\Delta\sigma_{Rsk}(N^*) = 58.5$ MPa (welded rebars) is the stress range at $N^* = 10^7$ cycles which is determined from S-N curves in Figure 2.2. This ratio is compared to a damage equivalent stress range, $\Delta\sigma_{s,equ}(N^*)$.

$$\gamma_{F,fat} \cdot \Delta\sigma_{s,equ}(N^*) \leq \frac{\Delta\sigma_{Rsk}(N^*)}{\gamma_{s,fat}} \tag{2.9}$$

The damage equivalent stress range is calculated from (2.10) where $\Delta\sigma_{s,Ec}$ is the calculated stress range from LM3 for road bridges and LM71 for railway bridges and λ_s is the damage equivalent factor.

$$\Delta\sigma_{s,equ} = \Delta\sigma_{s,Ec} \cdot \lambda_s \tag{2.10}$$

The damage equivalent factor is composed by a number of $\lambda_{s,i}$ factors shown in (2.11). The $\lambda_{s,i}$ factors are calculated somewhat different depending on bridge type, i.e. road bridge or railway bridge. Road bridge calculations are presented next, however the significant parameters from S-N curves are the same regardless of bridge type.

$$\lambda_s = \phi_{fat} \cdot \lambda_{s,1} \cdot \lambda_{s,2} \cdot \lambda_{s,3} \cdot \lambda_{s,4} \tag{2.11}$$

ϕ_{fat} is a damage equivalent impact factor depending on surface roughness. $\lambda_{s,1}$ takes into account effects from element type and influence area and are prescribed in tables in EC2 [4b]. $\lambda_{s,2}$ is a factor considering traffic volume according

to (2.12).

$$\lambda_{s,2} = \overline{Q} \sqrt[k_2]{\frac{N_{obs}}{2.0}} \tag{2.12}$$

The quantity $\overline{Q}$ is traffic type and k_2 is the curve inclination after N^* cycles in appropriate S-N diagram. N_{obs} is the number of lorries per year tabulated in EC2. $\lambda_{s,3}$ denotes influence of service life according to (2.13).

$$\lambda_{s,3} = \sqrt[k_2]{\frac{N_{years}}{100}} \tag{2.13}$$

The quantity N_{years} is the design life of the bridge and k_2 as described earlier. $\lambda_{s,4}$ describes influence of multiple lanes according to (2.14).

$$\lambda_{s,4} = \sqrt[k_2]{\frac{\sum N_{obs,i}}{N_{obs,1}}} \tag{2.14}$$

$N_{obs,i}$ is the number of lorries per year on lane i and $N_{obs,1}$ is the number of lorries per year on the slow lane.

The interesting parameters which could be altered after experiment are $\Delta\sigma_{Rsk}(N^*)$ and k_2 and three conclusions can be drawn from studying above equations. Firstly, If the result exceeds provided S-N curves in the standard that implies a parallel shift of the S-N curve which increases $\Delta\sigma_{Rsk}(N^*)$. Secondly, curve inflection point, N^*, is important since an earlier shift between curve inclination k_1 and k_2 also would increase $\Delta\sigma_{Rsk}(N^*)$. Finally, if curve inclination after N^* cycles is more flat compared to the standard, an increased value of k_2 may be proposed.

2.6.2 Background to Fatigue Sections in Eurocode 2

When comparing fatigue design standards such as *Eurocode 3* [34a] for construction steel with *Eurocode 2* [3a] for reinforcing steel, some differences are noticed. Construction steel have an inclination of 3 until $5 \cdot 10^6$ cycles whereon the inclination changes to 5. For reinforcing steel the S-N curve for unaffected straight rebars have an initial inclination of 5 which changes to 9 at 10^6 cycles. This difference in performance can perhaps be explained by the difference in axial and bending tests where full scale bending tests of concrete beams ensure that fatigue failure in rebars occur where the concrete is cracked which not necessarily is where the rebar have the most flaws, see Section 2.5.5. For welded rebars, curve inclination is similar to ordinary construction steel, however inclination switch between 3 and 5 is set to 10^7 cycles which differs from construction steel.

The european code for concrete design was developed during the 1980'ies and is to an extent based on *fib Model Code* [5]. Linear elastic behaviour is assumed which gives too high calculated stresses compared to real stresses, thus conservative designs are obtained [11e]. Sections concerning fatigue verification were written in Germany thus some influence from German design standards of that time is incorporated. In short, the design S-N curves governing selection of $\Delta\sigma_{Rsk}(N^*)$ and N^* values are have been developed from experimental result analysis. Up to about $2 \cdot 10^6$ cycles the experimental basis is strong. After this, fewer studies are available and pragmatic selections are necessary [40].

For straight unaffected rebars the curve inclination before N^* cycles is probably a good fit. The selection of $N^* = 10^6$ is from the fact that inclination switch is somewhere in between 10^6 and $5 \cdot 10^6$ cycles yet no exact inflection point exists in reality. Curve inclination after 10^6 cycles is a conservative choice due to a smaller available pool of test result [40].

Welded rebars have different quantity values compared to unaffected rebars. Initial curve inclination of 3 inflects after 10^7 cycles. Whether good scientific background is available until 10^7 cycles is unclear. Welded rebars show high reduction in fatigue strength thus a conservative selection of N^* is not surprising. Few studies exist where rebars have been tested above 10^7 cycles and curve inclination after inflection is as well a pragmatic and conservative assessment [40].

2.7 Stress Calculations

To determine an acting stress field can be both simple and complex depending on selected method and component shape. *Nominal Stress Approach*, *Structural Hot Spot Approach* and *Effective Notch Stress Approach* are presented next which are common approaches.

The nominal stress is the stress in the considered area calculated with general theories of structural mechanics. When the *nominal stress approach* is applied, the stress is calculated in the sectional area under consideration. The local stress effects from welds are ignored. However, macrogeometric effects, stresses from concentrated loads and misalignments are to be included since both may cause significant redistribution of section stresses [17b]. When these effects are included, a modified nominal stress can be calculated which is the bases for design. Fatigue resistance S-N curves of classified structural details in e.g. EC3, are based on the nominal stress approach [17c].

A structural hot spot is a point where a fatigue crack may initiate in the structure due to structural stresses, weld geometry and notches. The weld profile itself is excluded [17d]. Commonly the structural hot spot approach is applied when no clearly defined nominal stress can be identified due to complicated geometry or when the structural discontinuity is not comparable to a classified detail. The use of structural hot spot generally requires a finite element analysis (FEA) of the detail [17e].

Assuming linear-elastic material behaviour, the effective notch stress is the stress calculated at the notch root. An effective weld contour is introduced in order to account for weld shape parameters and non-linear material behaviour at the notch root [17f].

2.8 Statistical Evaluation Theory

Fatigue testing exhibits a significant variation in test results although testing procedure is well controlled [41]. A fundamental assumption is a log-normal distribution of experimental results for each stress range since experimental error can origin from a vast number of sources. Sampling averages tend to be normal distributed even though individual errors or result are not which is the basis for the *the central limit effect* in statistics [42a]. Statistical approach is

examined in detail in Section 3.4.

2.9 Discussion

Brittle and ductile materials show different fatigue properties, where ductile material is less affected by cyclic loading. Since the tested K500C-T rebars are manufactured by TEMPCORE processing hence providing a ductile core which hopefully remains sufficiently unaffected by the welding, one possibility is that fatigue life is preserved. The outer, more brittle, martensitic zone will probably be affected by the welding, thus the question remains; to what extent the heat affected zone will penetrate the rebars. Since the welding is performed by industrial robots, the welds will be, more or less, identically executed, which entails that variances of weld spots and heat affected zones are expected to be negligible.

Tilly [1] reported that an increase in steel grade above 420 MPa did not increase fatigue strength of rebars. Zheng and Abel [19] contradict this, in some way, stating that fatigue resistance of rebars are strongly dependent on the tempered martensitic outer layer. The martensite shows high fatigue resistance and once this layer fails the core material of mainly ferrite crystals fails relatively quickly. It is suggested that fatigue mainly starts in ferrite crystals and when the martensite fails, there is not much fatigue resistance left in the fatigued core of a QST rebar. For the testing herein this could implicate that fatigue life is reduced if the martensite layer is destroyed or altered by the welding.

The main expectation of the testing herein, is that welding only has minor effect on the fatigue performance, since non load-carrying welds are examined where the tested longitudinal rebars fatigue life reduction, hopefully will show to be low. As Section 2.5.3 and 2.5.4 describes, welding will to some extent decrease the fatigue life, however a common finding in literature is also that fatigue life of tested specimens with non load-carrying attachments, as reinforcement crossings or cruciform specimens, presents higher fatigue endurance when compared to design standards.

Fatigue life and behaviour of steel in general is studied in great extent and a vast amount of different studies is available. The steel construction trade has traditionally been more impelled to consider fatigue issues since fatal accidents have occurred where causation to fatigue failure are very likely. For instance, the first commercial jet airliner, *the Comet*, had several disasters originating from fatigue failure, which at the time of the 1950'ies not was fully comprehended [15a]. In infrastructure engineering the safety margins are in general higher when compared to the vehicle industry and complete collapses entirely caused by fatigue have never been reported [2]. Nevertheless, as the structures slenderness increases along with material optimization and more frequent and heavier traffic, fatigue issues appear.

When narrowing down the research area to reinforcing steel for concrete the field of course diminished but is yet large. Many fatigue studies are performed on reinforcement bars, both in air and in concrete and overview articles and state of the art reports have been published, e.g. [1, 2].

Welding of reinforcing steel for concrete when it comes to fatigue behaviour, is studied, however not that many studies are available. Available literature is moreover frequently focused on load-carrying butt-welded details, which by no

means are comparable to tests herein. A few studies have been performed quite similar to the ones of this scope, showing the importance of separating butt-welding and spot- or tack welding. In design standards, e.g. EC2 or MC2010 [3, 5], welded bars are all treated the same irregardless of to what extent the welding procedure has affected the rebar. Furthermore, no distinguishing is made between load-carrying and non load-carrying welding in design standards.

Judging by that EC2 was mainly written in the 1980'ies and keeping in mind the limited number of fatigue tests performed on QST rebars in present day (and hence also in the 1980'ies) a probability might be that S-N curves not necessarily are representative for QST rebars, which also is pointed out by Zheng and Abel [19]. Since present design models do not include microstructure properties, there might thus exist a gap between Eurocode 2 and the research field as well as material development.

Chapter 3

Method

Fatigue tests of rebars with a *stress-life* approach has been conducted. Main objectives of experiment and specimen descriptions will be examined as well as loading specifications. Furthermore, statistical approach for result analysis is also treated and a short hypotheses is presented next.

A brief overview of available standards for fatigue testing and succeeding statistical evaluation was performed. Testing standards were not followed to the letter, however they were used as guidelines when testing procedure was drawn.

3.1 Objectives and Scope

In order to properly evaluate fatigue behavior of robot welded reinforcement bars, an experiment was performed and the result was compared to reference S-N curves from EC2 [3c], see Figure 2.2. In total, 23 specimens were tested axially in air by cyclic loading with constant stress range until catastrophic failure and the result was statistically analyzed. As discussed in Section 2.6.1, three main possibilities exist in order to affect the design standard: show parallel shift of the design curve, i.e. test result exceeds current S-N curve in EC2 *and/or* present a curve inclination switch earlier than current $N^* = 10^7$ cycles *and/or* indicate that present curve inclination after infection point, N^*, is more flat than currently prescribed.

3.2 Specimen Description

A specimen from two pieces of different rebars were welded together. Geometry and material characteristics are presented next.

3.2.1 Specimen Geometry

A total of 25 specimens were manufactured by an industrial procedure where two pieces of reinforcing steel, with length of 600 mm and 100 mm, were welded together by robots according to Figure 3.1 and Figure 4.3. The diameter of the longitudinal rebar was ϕ20 mm and the shorter transversal rebar was ϕ16 mm. The welding method was MAG135 which is a standard welding method

according to [43b, c]. The length of 600 mm was chosen from the suggestion in [2d] where it is stated that the specimen length should be 30 times the nominal diameter of the rebar, as calculated in (3.1).

$$L = 30 \cdot 20 \text{ mm} = 600 \text{ mm} \tag{3.1}$$

In [43c] a ratio condition between minimum and maximum bar diameter is also specified according to (3.2), which also is met.

$$\frac{\phi_{\min}}{\phi_{\max}} \geq 0.4; \qquad \frac{16}{20} = 0.8 \geq 0.4 \Longrightarrow \text{OK}. \tag{3.2}$$

A specimen was subsequently installed in a testing machinery as shown in Figure 3.3. Cyclic loading was applied according to Section 3.3.

3.2.2 Specimen Material

The reinforcing steel was of *K500C-T* type, a common steel type in infrastructure constructions in Sweden. It is a ribbed steel with yielding strength of 500 MPa together with a QST manufacturing process, described in Section 2.5.1. The explicit steel composition is presented in Table 3.1.

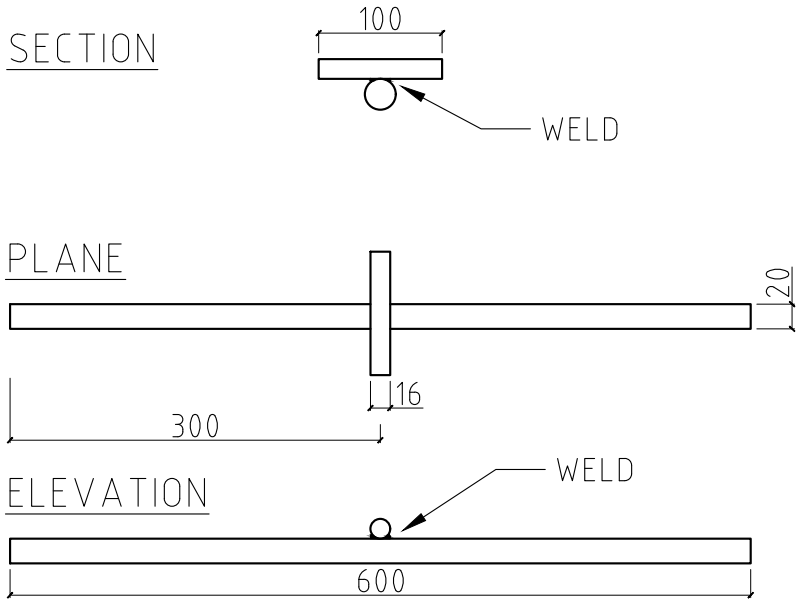

Figure 3.1: Specimen design.

(a) Overview of a specimen.

(b) Picture showing spot weld.

(c) Picture showing welded connection between rebars.

(d) Picture showing welded connection between rebars.

Figure 3.2: Pictures of a specimen before testing.

Table 3.1: Steel composition for K500C-T used in the experiment, by weight percent. CE1 and CE2 are carbon dioxide equivalents.

C	Max	0.204		Si	Max	0.250		Mn	Max	1.050
	Aim	0.190			Aim	0.170			Aim	1.000
	Min	0.170			Min	0.150			Min	0.950
P	Max	0.035		S	Max	0.030		N	Max	0.012
	Aim	-			Aim	0.020			Aim	-
	Min	-			Min	-			Min	-
Cr	Max	0.400		Ni	Max	0.400		Al	Max	-
	Aim	-			Aim	-			Aim	-
	Min	-			Min	-			Min	-
Cu	Max	0.600		Mo	Max	0.100		Nb	Max	-
	Aim	0.500			Aim	-			Aim	-
	Min	-			Min	-			Min	-
Sn	Max	0.040		Pb	Max	-		Zn	Max	-
	Aim	-			Aim	-			Aim	-
	Min	-			Min	-			Min	-
V	Max	-		CE1	Max	-		CE2	Max	0.454
	Aim	-			Aim	-			Aim	-
	Min	-			Min	-			Min	0.355

Figure 3.3: Testing Machinery

3.3 Loading Specifications

An axial force controlled method for fatigue testing was adapted. The stress range was constant during each specific test series, however varied in between test series in order to develop a S-N curve. Initially a large stress range was selected whereat it gradually was reduced as shown in Table 3.2. Corresponding force range for a $\phi 20$ mm rebar calculated by *nominal stress approach* is also presented in Table 3.2. The longitudinal rebar was subjected to a sinusoidal varying force in order to obtain cyclic stresses and by extension fatigue of the material. Firstly, a quite high stress range of 280 MPa was selected in order to establish a rather quick result to be compared to design curves in EC2. From this result the next stress range was selected and gradually the stress ranges were lowered in order to maximize the number of total cycles, given provided machine time. 4 different stress ranges, 280, 176, 164 and 148 MPa, were evaluated with 5 specimens at each stress range as seen in Table 3.2. The last test series, of 148 MPa, contained 6 specimens because of available machine time.

Design according to EC2 is presented in Section 2.6.1. The curve inflection point is chosen to 10^6 cycles for unaffected rebars which corresponds to a stress range of 162.5 MPa. Thus the stress ranges of 176, 164 and 148 MPa were selected in order to evaluate if an inflection point could be found earlier than 10^7 cycles, which is the inflection point for welded rebars.

The temperature was constant at approximately 20° C and testing was performed at a frequency of 10-16 Hz. The variation of frequency is due to machine limitation where higher frequencies were possible to apply during lower stress ranges. Frequency effects are not present up until approximately 150 Hz, thus the varying frequency should not be of concern [2c].

3.3.1 Maximum Stress and Stress Ratio

As defined in Section 2.2, high cycle fatigue prescribes stresses within the elastic domain. It is necessary to avoid unacceptable plastic strains in the reinforcement, thus the elastic stresses should not exceed 80% of the characteristic value of the steel yield strength, as suggested in [44]. A common choice of stress ratio is 0.2 which also was adopted for the testing herein [2c]. Given a stress ratio 0.2 together with a characteristic rebar yield strength of 500 MPa results in a stress range limit of 400 MPa in order for $\sigma_{\max} \leq 500$ MPa thus avoiding yielding of the steel. From above reasoning, of maximum stress together with stress ratio, the maximum stress was chosen to 70% of the characteristic yield strength, $f_y = 500$ MPa, in order to be on the safe side of steel yielding, hence $\sigma_{\max} = 350$ MPa. As discussed in Section 2.1.5, the maximum stresses will decrease with

Table 3.2: Evaluated stress ranges with associated force ranges for a bar diameter of $\phi 20$ mm.

Specimen	$\Delta\sigma$ [MPa]	$F_{\max}$ [kN]	$F_{\min}$ [kN]
1-7	280	110.0	22.0
8-11,13	176	69.1	13.8
14-18	164	64.4	12.9
12,19-23	148	58.1	11.6

Table 3.3: Experimental loading values for each specimen as to *stress range*, *stress ratio*, *mean stress*, *max stress* and *min stress*.

Specimen	$\Delta\sigma$ [MPa]	R [-]	σ_{mean} [MPa]	σ_{max} [MPa]	σ_{min}[MPa]
1-7	280	0.200	210	350	70
8-11,13	176	0.200	132	220	44
14-18	164	0.200	123	205	41
12,19-23	148	0.200	111	185	37

the lowering of stress range, given a constant stress ratio. Table 3.3 presents a clear view over σ_{mean}, σ_{max} and σ_{min} where the decrease is obvious.

3.3.2 Definition of Failure and Run-out

Specimens were tested until complete failure, i.e. separation into two parts. In accordance with [45], any failure occurring within the distance of $2\phi = 40$ mm or closer to the machine grips, that particular specimen is to be considered as invalid. Specimen 2 and 3 failed at gripping areas and were hence omitted from analysis. Testing was aborted if a specimen survived more than $1.6 \cdot 10^6$ cycles which was the case for specimen 12. Specimen 12 was also excluded from analysis which is discussed in Chapter 5.

3.4 Statistical Analysis of the Results

After failure, each test was examined in more detail. A test file was produced by the testing machine which displays a more precise test data as to *max deformation*, *min deformation*, *max force*, *min force* and *frequency* connected to a specific *loading cycle*. Needless to say, the test files are large, measured in rows, and are hence not included in the appendix.

Exact stress range, stress ratio and fatigue life were gathered from the test file and stress range to fatigue life could be displayed graphically in a log-log plot, see Chapter 4.

The mathematical formulations regarding statistical evaluation of the test result are presented in Section 3.4.1 which in all essence follows ISO-12107 [41]. A linear regression curve is drawn and the corresponding 5% fractile is compared to present design curves in EC2 [3a].

3.4.1 Linear Regression

As mentioned in Section 2.2.1, Basquin was first to suggest the well-known power law to properly describe fatigue life, see (3.3), where N_f is the fatigue life in number of stress cycles, $\Delta\sigma$ is the applied stress range and k and C are material constants.

$$N_f \Delta\sigma^k = C \tag{3.3}$$

By using logarithms (3.3) becomes linear, as shown in (3.4).

$$\log N_f = \log C - k \log \Delta\sigma \tag{3.4}$$

According to (3.3) and (3.4), the logarithms of the tested stress ranges and the corresponding logarithmic fatigue lives were calculated. Furthermore, the curve inclination coefficient k and the ordinate crossing C were established, as per (3.5) and (3.6), in order to describe a linear curve in log-scale where n is the number of specimens which in this case is $n = 20$.

$$k = \frac{\sum_{i=1}^{n} \log \Delta\sigma_i \log N_{f,i} - \frac{\sum_{i=1}^{n} \log \Delta\sigma_i \sum_{i=1}^{n} \log N_{f,i}}{n}}{\sum_{i=1}^{n} (\log \Delta\sigma)^2 - \frac{\left(\sum_{i=1}^{n} \log \Delta\sigma\right)^2}{n}} \tag{3.5}$$

$$\log C = \frac{\sum_{i=1}^{n} \log N_{f,i} - k \sum_{i=1}^{n} \log \Delta\sigma_i}{n} \tag{3.6}$$

With the parameters, k and $\log C$ defined, the stress ranges from the test series are used in the new formulated linear equation (3.7) and from this equation, *predicted* fatigue lives, $N_{f,\text{predic}}$, can be calculated. The predicted fatigue lives are plotted against the stress ranges which of course forms a linear curve in log scale, i.e. a linear regression curve.

$$\log N_{f,\text{predic}} = \log C - k \log \Delta\sigma \tag{3.7}$$

The characteristic value is defined as the lower tolerance limit of the statistical 5% probability of failure, $P = 5$, on a 75% confidence interval, $1 - \alpha = 75$, i.e the 5% fractile. In order to determine a 5% fractile curve corresponding to currently established linear regression curve in (3.7), a standard deviation, s, is calculated according to (3.8) where p is the number of estimated parameters, i.e. k and $\log C$ thus in this case $p = 2$.

$$s = \sqrt{\frac{\sum_{i=1}^{n} (\log N_i - \log N_{i,\text{predic}})^2}{n - p}} \tag{3.8}$$

For a linear case, the predicted lower tolerance fatigue life, $N_{f,\text{predic},5\%}$, is calculated as shown in (3.9) where v is the number of degrees of freedom, $v = n - p$ and $\overline{\Delta\sigma}$ is the mean value of the applied stress ranges. For the case of a characteristic value defined as above, $k_{P,1-\alpha,v} = k_{5,75,18}$, which is the characteristic fractile factor and is selected from *Annex D - Design Assisted by Testing* in *EC0* [46]. For the testing herein $k_{5,75,18} = 1.760$.

$$\log N_{f,i,\text{predic},5\%} = \log N_{f,i,\text{predic}} - k_{P,1-\alpha,v} \cdot s \left[1 + \frac{1}{n} + \frac{(\log \Delta\sigma_i - \log \overline{\Delta\sigma})^2}{\sum_{i=1}^{n} (\log \Delta\sigma_i - \log \overline{\Delta\sigma})^2}\right]^{\frac{1}{2}} \tag{3.9}$$

From the result provided by (3.9), the characteristic curve can be calculated and plotted which is shown in Chapter 4.

In order to evaluate statistical assumptions, as to a log-normal distribution of test result, correlation coefficient and residual plots are calculated and shown. Correlation coefficient, R^2, for the linear regression is calculated according to (3.10) and describes the linear regression fit, to actual test result. A correlation coefficient value of above 0.9 is desirable and indicates a good fit [41].

$$R^2 = \frac{\left(\sum_{i=1}^{n} \log \Delta\sigma_i \log N_i - \frac{\sum_{i=1}^{n} \log \Delta\sigma_i \sum_{i=1}^{n} \log N_i}{n}\right)^2}{\left(\sum_{i=1}^{n} (\log \Delta\sigma_i)^2 - \frac{\left(\sum_{i=1}^{n} \log \Delta\sigma_i\right)^2}{n}\right)\left(\sum_{i=1}^{n} (\log N_i)^2 - \frac{\left(\sum_{i=1}^{n} \log N_i\right)^2}{n}\right)} \tag{3.10}$$

The residual, e, is the distance from actual tested fatigue life, N_f, to the predicted fatigue life, $N_{f,\text{predic}}$, as shown in (3.11). The residuals are plotted against predicted fatigue life and the residuals should be distributed evenly around 0. This also implies that the sum of the residuals are zero [41].

$$e_i = \log N_{f,i} - \log N_{f,i,\text{predic}} \tag{3.11}$$

3.5 Optical Microscope

In order to distinguish fatigue stages, described in Section 2.4, an optical microscope was used on fracture surfaces. Different fatigue specific surface appearances were also looked for and in Chapter 4 pictures are available.

3.6 Hypotheses

Welding affects the fatigue resistance of reinforcement bars highly. However, consideration was put into minimizing the effect of the welding by introducing welds performed by industrial robots. Consequently the test outcome should be somewhere in between earlier test results of tack welded reinforcement bars and unaffected rebars. The experiments will be carried out on *as received bar* in air. This would imply lower fatigue life as discussed in Section 2.5.5. In summary, by introducing robots a possibility of enhanced fatigue life appears however the welding will still affect fatigue life negatively. Additionally, testing in air is known to produce inferior result.

There is also risk of introducing high local stresses at the areas where the machine is gripping the specimen causing premature fracture at the ends of the specimen. The hypothesis is however that the fracture will be in the center part of the specimen since the welding procedure introduce brittle material behaviour as well as stress concentrations [1, 44].

Chapter 4

Results

As described in Section 3.3, 4 different stress ranges, 280, 176, 164 and 148 MPa were chosen for the experiment. Due to machine characteristics and small variations in steel geometry and material properties, the desired stress range was not exactly matched during testing. As can bee seen in the following result-tables and figures, the actual obtained stress range varied somewhat thus a distribution is seen between stress ranges even though the objective was to minimize differences in stress range within a test series.

An overview of test result is presented next with tables and figures. Thence fracture surfaces which have been examined by optical microscope is presented with pictures. Furthermore, the result of the statistical analysis is shown.

4.1 Result overview

The first tested stress range at 280 MPa is seen at the top of Figure 4.1 and an enlargement of that specific region is visualized in Appendix A.1, Figure A.2. Specific test result for each specimen is shown in Table 4.1. No remarkable outcome is seen and fatigue life is close to estimated life according to S-N curve for welded rebars in EC2 [3c].

When the stress range was lowered to 176 MPa, the same trend is obvious, as seen in Figure 4.1. The test results displays good agreement to present design curve and is also presented in Table 4.2.

The next stress range of 164 MPa shows no change in trend. The fatigue life is still in resemblance with design curve and is displayed in Table 4.3.

For the stress range of 148 MPa one specimen exhibited fatigue life of over $1.6 \cdot 10^6$ cycles and the testing was, due to time issues, aborted. However, after further testing at this stress range it seems as this was only a particularly strong specimen and remaining specimens failed yet again in good agreement with the design curve for welded rebars from EC2 [3c]. The result at the stress range of 148 MPa is shown in Table 4.4.

Additional figures are available in Appendix A.1 as to larger and smaller scales in order to illustrate the result further.

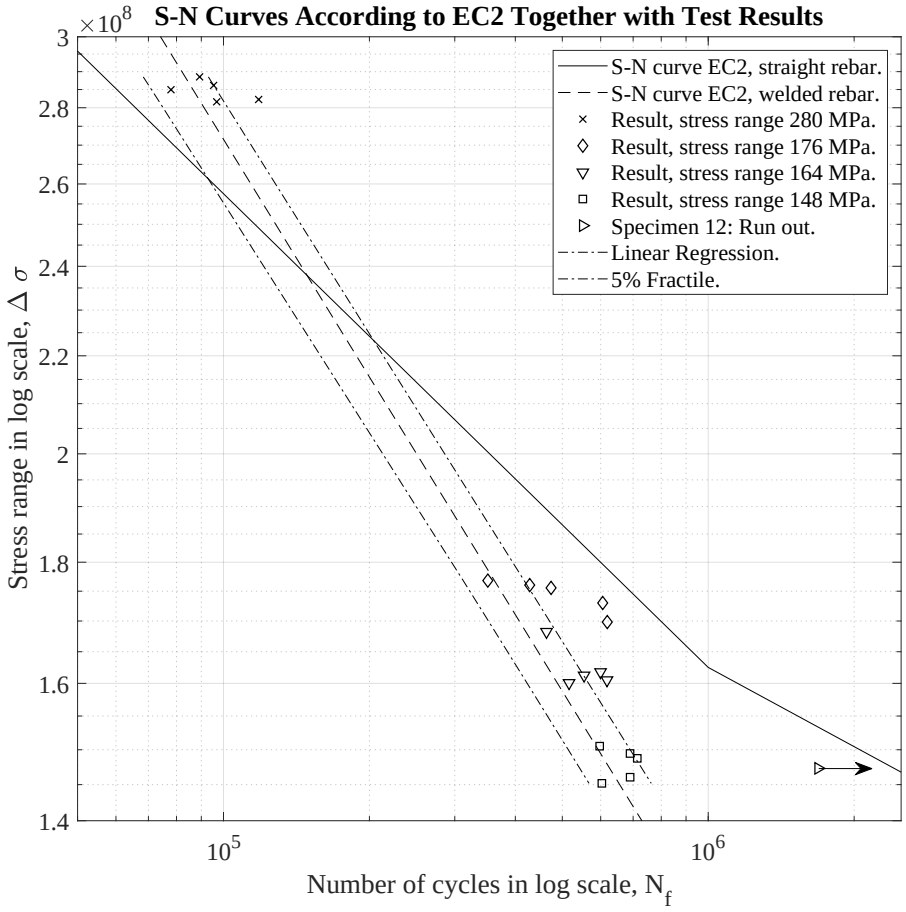

Figure 4.1: S-N curves from EC2 together with test results. Linear regression curve and corresponding 5% fractile is also shown.

Table 4.1: Test series 1. Aimed stress range 280 MPa.

Specimen	Stress Range, $\Delta\sigma$, [MPa]	Life, $N_f \cdot 10^3$	Freq. [Hz]	Stress Ratio
1	286	89	10	0.1854
4	285	78	10	0.1913
5	282	97	10	0.1955
6	286	95	10	0.1907
7	282	118	10	0.1969
Mean	285	96	-	0.1919

Table 4.2: Test series 2. Aimed stress range 176 MPa. (*Frequency was lowered after $481 \cdot 10^3$ cycles.)

Specimen	Stress Range, $\Delta\sigma$, [MPa]	Life, $N_f \cdot 10^3$	Freq. [Hz]	Stress Ratio
8	177	351	10	0.1940
9	176	428	16	0.1966
10	170	619	16-10*	0.2137
11	173	605	12	0.2159
13	176	474	12	0.1974
Mean	174	496	-	0.2035

Table 4.3: Test series 3. Aimed stress range 164 MPa.

Specimen	Stress Range, $\Delta\sigma$, [MPa]	Life, $N_f \cdot 10^3$	Freq. [Hz]	Stress Ratio
14	161	554	15	0.2083
15	168	464	15	0.1875
16	162	600	15	0.2064
17	160	516	15	0.2114
18	161	618	15	0.2102
Mean	162	550	-	0.2048

Table 4.4: Test series 4. Aimed stress range 148 MPa. (*Run out. Test was aborted without failure and fatigue life is not included in mean value or statistical analysis)

Specimen	Stress Range, $\Delta\sigma$, [MPa]	Life, $N_f \cdot 10^3$	Freq. [Hz]	Stress Ratio
12	147	1686*	15	0.2051
19	146	690	15	0.2027
20	145	603	15	0.2098
21	151	597	15	0.1923
22	149	690	15	0.1959
23	149	714	15	0.1982
Mean	148	659	-	0.1998

4.1.1 Statistical Analysis

The result was examined with statistical analysis where a linear regression curve and corresponding 5% fractile curve was produced, which is seen in Figure 4.1. Furthermore, correlation coefficient, R^2, and slope inclination, k_1, were calculated and compared to design standard. The procedure is discussed in detail in Section 3.4.

The correlation between linear regression curve and actual test result was good and approximately $R^2 = 0.97 \geq 0.9$. The slope of calculated curves were approximately $k_1 = 3.1$ which is somewhat better than the prescribed value of 3 in EC2 [3d]. Table 4.5 show these calculated values.

The residual plot is presented in Figure 4.2, where result distribution in general is good. Two test result show some slight deviation from other residuals, see the top most points in Figure 4.2.

Specimen 12 was excluded from the statistical analysis.

Table 4.5: Correlation coefficient R^2 and slope inclination, k_1.

R^2	k_1
0.9682	3.0631

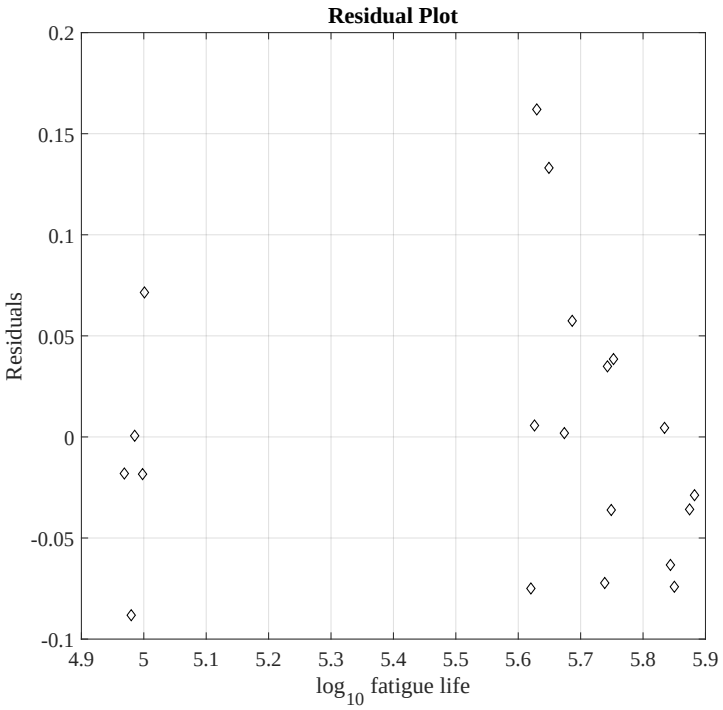

Figure 4.2: Residual plot with logarithmic scale.

4.2 Fracture Surfaces

The fatigue phases, as discussed in Section 2.4, were studied by eye and optical microscope. As seen in Figure 4.3c and Figure 4.3d, crack initiation is located in the weld vicinity. The crack opening produce characteristic large orthogonal cracks to propagation direction. When crack initiation have occurred, the crack propagates, creating a smooth area until stresses are to intense and sudden brittle fracture separates the specimen. The brittle fracture area is seen as rough and jagged in Figure 4.3.

Fracture surfaces from specimens 1 and 10 were also studied with optical microscope and pictures are presented below, see Figure 4.4. In Figure 4.4a and Figure 4.4b differences in surface roughness may be seen when the the fractures are studied. The martensite shell can also be seem, however with some difficulty. The heat affected zone is seen as a lighten parabola, striking through the martensite. Figure 4.4c is a magnification of the crack initiation site of specimen 10. Larger cracks which spread from the edge of the surface into the steel can be seen. Next, Figure 4.4d show a banded structure from the centerpiece of specimen 10 fracture surface. This banded structure could be slip bands as discussed in section 2.3.3. Finally, Figure 4.4e and Figure 4.4f, are representations of different propagation areas on the surface of specimen 10. Figure 4.4e show a rough and wavy surface at the end of propagation phase, before fracture and Figure 4.4f is an enlargement of early propagation which show a more smooth surface nature.

(a) Fracture surface of specimen 1.

(b) View of separation of specimen 1.

(c) Fracture surface of specimen 9.

(d) Fracture surface of specimen 16.

Figure 4.3: Pictures of a specimens after testing.

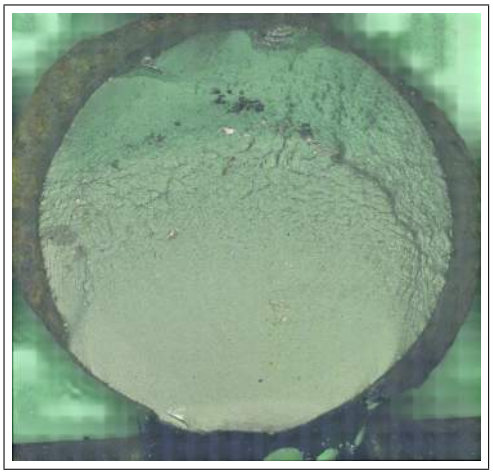

(a) Picture of fracture surface from specimen 10 from optical microscope.

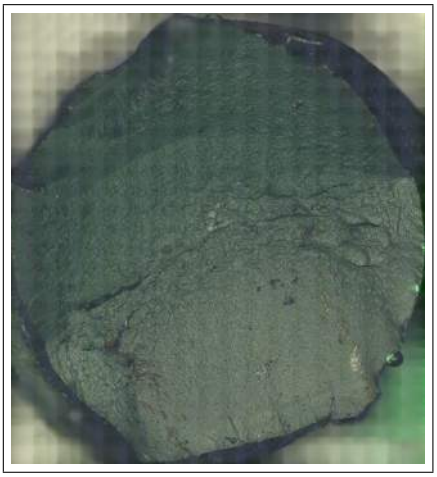

(b) Picture of fracture surface from specimen 1 from optical microscope.

(c) Picture of crack initiation site for specimen 10 from optical microscope.

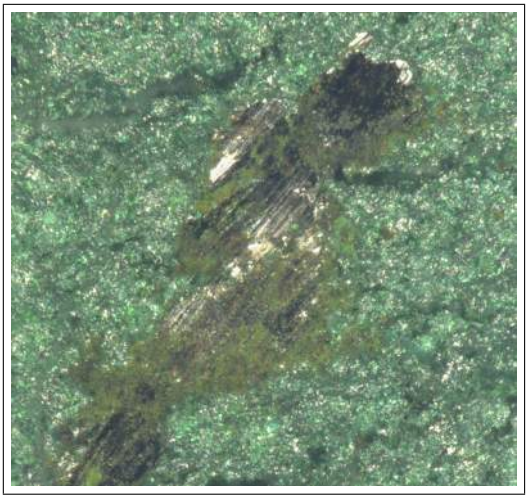

(d) Captured banded structure from center of fracture surface of specimen 10.

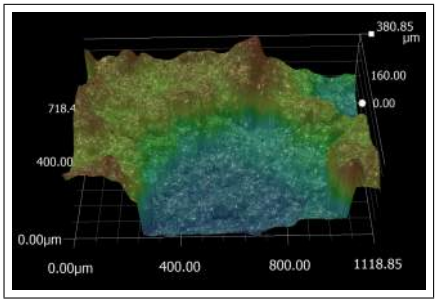

(e) Rough surface just before brittle failure zone of specimen 10.

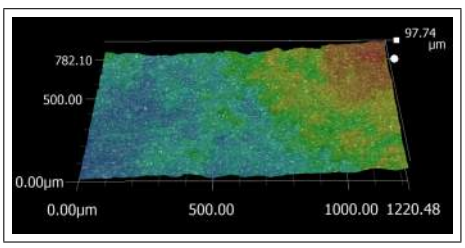

(f) Smooth zone at the beginning of propagation zone of specimen 10.

Figure 4.4: Picture from optical microscope.

4.3 Propagation Phase

After crack initiation, the crack starts to propagate, see Section 2.4. The crack propagation phase is seen clearly if deformation is visualized in relation to matching cycle. In Figure 4.5, the last $80 \cdot 10^3$ cycles is seen, one curve from each stress range. The propagation starts where the deformation starts to increase quickly however a precise demarcation can not be determined. It is obvious that once crack is initiated, the propagation phase is rather quick and fracture occur rapidly. A small difference can be seen between stress ranges where a lower stress range seem to show a slightly longer propagation phase.

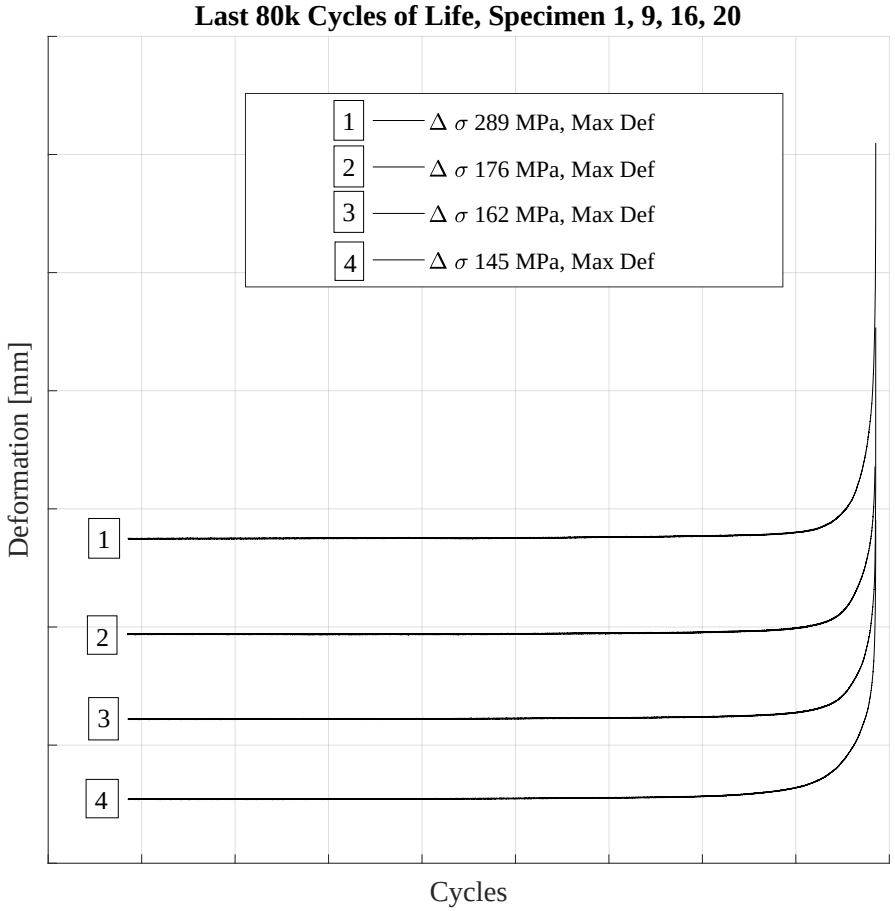

Figure 4.5: Last $80 \cdot 10^3$ cycles from 4 different stress ranges. The curves are moved in the plane in order to enable a comparison, hence no axis values are shown.

4.4 Problems During Testing

Specimen 2 and 3 suffered from failure at machine gripping areas. This was probably because of gripping over ribbing area of the rebar introducing high stress concentrations to the ribs. When the rebar was rotated providing a larger area on which the jaws clamped, this problem was avoided and apart from specimen 2 and 3 all specimens failed at the vicinity of the welded zone.

(a) Crack at gripping area. Machine jaw marking just over ribbing area.

(b) Good gripping markings.

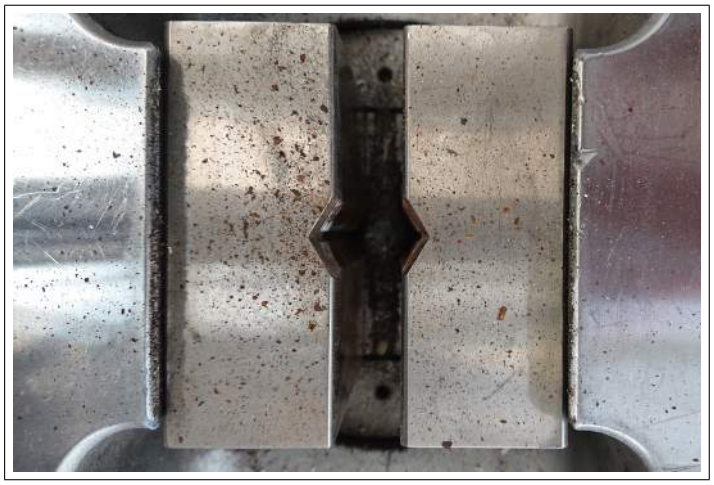

(c) Pictures of machine gripping jaws.

Figure 4.6: Specimen orientation influence.

Chapter 5

Discussion

An overall discussion of the test results is initially held whereby conclusions are presented and finally future research is proposed.

5.1 Results

Initially the test results regarding the rebar microstructure is discussed in relation to Chapter 2. Furthermore, Eurocode 2 and the testing outcome are compared and reviewed and finally method and relevant implications are discussed.

5.1.1 Reinforcement Bar Microstructure

Crack initiation occurred in the vicinity of the weld where the heat affected zone has destroyed the harder martensite, as may be seen with some difficulty in Figure 4.3 and Figure 4.4. As discussed in Section 2.5, the rebar steel is mainly composed of martensite and ferrite. The martensite, a BCT unit cell structure, shows a semi-ductile behaviour and is harder compared to the ferrite. It is mainly the martensite which provides the high yield strength of 500 MPa, thus the martensite is a necessity. As suggested by Zheng and Abel [19] it seems as the tempered outer shell of martensite is an important factor of fatigue resistance. This is not surprising since it is well established that fatigue is a surface phenomenon implying that the material closest to the surface is highly relevant. Whether ductile or semi-ductile materials are beneficial in relation to fatigue is a relevant question and not fully clear. When cracks are initiated at the martensite surface, the cracks cut through the semi-brittle martensite zone more or less momentarily. Once this has occurred, the cracks start to propagate. As can be seen in Figure 4.5, when propagation has started, catastrophic failure is close. This underlines the importance of surface conditions and to have a steel of good fatigue resistance.

When unaffected QST rebars are tested in fatigue, for instance by Zheng and Abel [19] or Rocha et al. [25], the results are in good relation to the standards and other types of steel. This indicates that martensite may show more fatigue resistance in comparison to ferrite. The heat affected zone from the welding procedure, most likely destroys the martensite, whereafter a complex zone of

varying microstructure is the outcome. Overview articles and state of the art reports reviewed in this thesis, are from the 1980'ies. The reviewed articles are highly relevant because the field has not had any revolutionary new findings since the 1980'ies. However, QST rebars have shown to outperform older types of rebars in fatigue testing [19], thus newer steel types may show different fatigue performance in comparison to presented data in *Fatigue of Steel Reinforcement bars* [1] and *Bulletin 188* [2].

5.1.2 Eurocode 2

When the design standard, EC2, is studied it is obvious that stress ratio and mean stress are disregarded even though their relevance is well supported. As mentioned in Section 2.1.3, a probable cause is stress concentrations which reduce these effects. To what extent, remains unclear thus further testing where these parameters are altered could also endorse or disfavor current neglecting of mean stress and stress ratio effects.

As described in Section 2.6.1, the two relevant components are, k_2 and $\Delta\sigma_{Rsk}$, when it comes to fatigue design according to EC2 [4b]. If a result indicates that the design S-N curve for welded rebar was too conservative an argument could be made of an enhancement of present value of $\Delta\sigma_{Rsk}$ from a parallel shift of the design curve. The tested stress ranges in the present work, are in the interval of 280 to 148 MPa. The test results indicate a good fit to present design curve, thus no parallel shift can be suggested.

Since the $\Delta\sigma_{Rsk}$ quantity is selected at the curve inflection point, i.e. the stress range at which the curve inclination changes, there is a great value in determining this point more precisely. As may be seen for specimen 12, see Figure 4.1 or Table 4.4, a curve inclination switch could have been the case. Specimen 12 was the first test at 148 MPa and showed promising result. After testing all specimens at the stress range of 148 MPa, it is more likely that specimen 12 was an outlier, when compared to other tests at that stress range. The curve inclination switch is in general between 10^6 and 10^7 cycles [40]. Testing where the stress range is reduced further is necessary in order to pinpoint the exact inclination switch. The S-N curves in EC2 [3c] are based on a pragmatic choice, where reliable experimental background is available up to approximately $2 \cdot 10^6$ cycles. A conservative curve inclination is thus chosen after this point. If a more precis inflection point could be defined this could enhance the $\Delta\sigma_{Rsk}$ quantity. Current inflection point for welded rebars are set to $N^* = 10^7$ cycles. If the curve inflection point is shown to appear earlier than 10^7 cycles, this would thus increase $\Delta\sigma_{Rsk}$.

Further testing at lower stress ranges from 140 to 50 MPa would be most valuable since it would provide an actual curve inclination approximation. The curve inclination after $2 \cdot 10^6$ cycles is a conservative approximation and a more complete investigation could result in an increased k_2 value. When stress ranges are reduced, experimental scatter is known to increase, thus numerous tests are necessary at each stress range.

As may be seen in Figure 5.1, the curves of unaffected and weld affected rebars diverge rapidly after 10^6 loading cycles from the inclination change for unaffected rebars. Testing at these stress ranges are highly interesting since it would show if the present curve for welded rebars is a good fit at these low stress ranges or a parallel shift to the right could come in question. Since less research

is available at these lower stress ranges, a chance might be that the pragmatic assessments are *too* conservative.

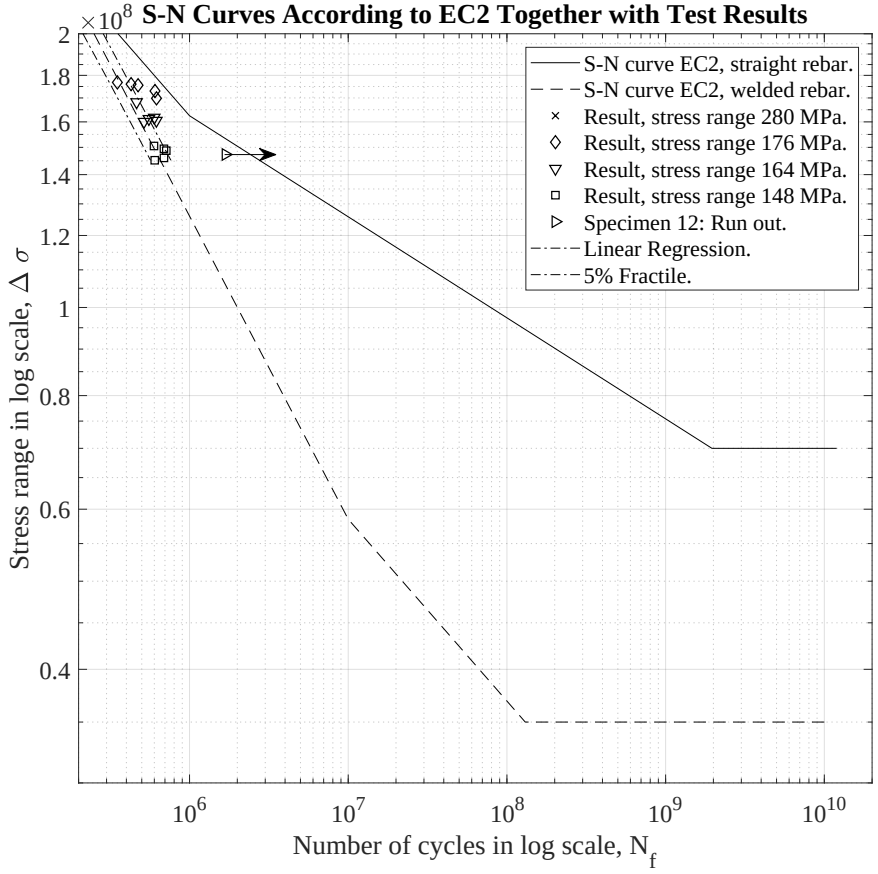

Figure 5.1: S-N curves from EC2 together with test results showing lower stress ranges and the area where design S-N curves for weld affected and unaffected rebars diverge.

In summary of the above, more testing is necessary in order to obtain N^* and the curve inclination k_2 more precisely. This requires testing where fatigue life is in the range of 10^6 to 10^8 cycles thus very long testing time.

5.1.3 Method of Testing

There is a large jump in tested stress range between 280 and 176 MPa. From earlier knowledge (c.f. [2]) it is reasonable to assume a linear relation over this interval and a test series in an intermediate stress range would most likely yield test results matching the S-N curves from EC2 as seen for the tested stress ranges.

Two specimens (2 and 3) suffered from grip failure and were excluded from the results and the succeeding statistical analysis. It was concluded from the gripping pattern over the rebars, that the machine jaws should be applied over

the flattest area of the rebars, c.f. Figure 4.6. A probable explanation is that when the gripping was centered directly over the ribs (as were the case for specimen 2 and 3) and not on the more flat area of the rebar, high local stresses were introduced to the ribs. When testing proceeded, the ribs suffered from small rotation from the back and forth motion produced by the testing machine. By extension, the rotational movement of the ribs, reduced the nominal elongation of the specimen thus also the stresses at the welded zones.

The testing was performed in air which do show conservative test results. If the experimental program had been performed by bending of RC-beams, the results would probably have been more favorable. It is however somewhat deceptive to suggest that testing in air presents incorrect results when compared to the *standard*. When the standard was written, test results from a vast amount of experiments were gathered, where a majority are performed in air. Hence, the design S-N curves are mostly influenced from testing in air and the comparison with the test results herein is from this inference most relevant.

5.2 Conclusions

The general findings are that the present design S-N curve in EC2 [3c] is representative for MAG135 welded rebars performed by industrial robots. Furthermore, EC2 has good scientific support for design S-N curves up until $2 \cdot 10^6$ cycles, whereafter a pragmatic assessment is the background to the design S-N curves. Thus, it is concluded that

- MAG135 welds performed by industrial robots presents no design advantage as to allowable stress ranges.
- The standard relies on good experimental background up until $2 \cdot 10^6$ cycles.

5.3 Future Research

Several interesting questions arise from the test results. The martensite is probably destroyed by the welding and a different welding method may be evaluated further. The heat affected zone seen at the specimen fracture surface was rather deep and perhaps a different welding method may interfere less with the steel. The martensite may be a steel of high fatigue resistance and to preserve the martensite shell with a less deep heat affected zone may be advantageous.

When large steel beam elements are manufactured, different post treatment of welds are performed in order to minimize the residual stresses. It may be of interest if similar techniques can be applied on spot welds and hence enhance fatigue life.

A completely different joining technique, other than welding, may also be in question and should be examined. For instance, high-end component adhesive can perhaps be an interesting new topic, since this may impact the steel less than welding.

A profound investigation of steel material could pave the way for a better understanding of important fatigue properties. Whether it is beneficial to have

a semi-ductile hard material or it actually is better if it is a more ductile remains to be shown.

Further lowering of the stress ranges should also be tested in order to establish the entire S-N curve. This would provide knowledge of where the S-N curve inflects and the succeeding curve inclination and by extension precise values of $\Delta\sigma_{Rsk}$ and k_2.

5.4 Final Remarks

As described in the introduction, Section 1.1, a major possibility lies in an automated processes of constructing reinforcement units. Great time reducing operations, such as the present initiative of a reinforcement station, play a major role concerning costs of infrastructure construction. Assembling reinforcement units with welding requires further testing which is time consuming and hence the costs are high. Collaboration between several companies and stakeholders are probably a path forward which already have begun.

The automatization has probably only began and technical solutions will most likely develop towards less human interference.

Bibliography

[1] Tilly, G.P. "Fatigue of Steel Reinforcement Bars in Concrete: A Review." In: *Fatigue & Fracture of Engineering Materials & Structures* 2.3 (1979), pp. 251–268. ISSN: 8756758X.

[2] CEB, Bulletin 188. *Fatigue of Concrete Structures. State of the Art Report.* Tech. rep. Lausanne, 1988.
a) *Section 1.1.*
b) *Section 1.3.*
c) *Section 4.1.*
d) *Section 4.1.1.1.*
e) *Section 4.1.1.2.*
f) *Section 4.1.1.3.*
g) *Section 4.1.1.4.*
h) *Section 4.1.2.3.*
i) *Section 4.1.3.2.*

[3] *SS-EN 1992-1-1:2005. Eurocode 2: Design of Concrete Structures - Part 1-1: General Rules.* 1st ed. Swedish Standards Institute, 2005.
a) *Section 6.8.*
b) *Section 6.8.4.*
c) *Figure 6.30.*
d) *Table 6.3N.*

[4] *SS-EN 1992-2:2005. Eurocode 2 - Design of Concrete Structures - Part 2: Concrete Bridges - Design and Detailing Rules.* 1st ed. SSI - Swedish Standards Institute, 2005.
a) *Section 6.8.*
b) *Annex NN.*

[5] *fib Model Code for Concrete Strutures 2010.* fib CEB-FIP, 2013.
a) *Section 5.2.5.6.*
b) *Section 7.4.1.*

[6] *TRVFS 2011:12. Trafikverkets författningssamling.* Trafikverket. [In swedish], 2011.

[7] *TRVK Bro 11. Trafikverkets tekniska krav Bro. TRV 2011:085.* Trafikverket. [In swedish], 2011.

[8] *TRVK Tunnel 11. Trafikverkets tekniska krav Tunnel. TRV 2011:087.* Trafikverket. [In swedish], 2011.

[9] *TRVR Bro 11. Trafikverkets tekniska råd Bro. TRV 2011:086.* Trafikverket. [In swedish], 2011.

[10] *TRVR Tunnel 11. Trafikverkets tekniska råd Tunnel. TRV 2011:088.* Trafikverket. [In swedish], 2011.

[11] Elfgren, L. *Fatigue Capacity of Concrete Structures. Assessment of Railway Bridges.* Tech. rep. Division of Structural Engineering, Department of Civil, Environmental and Natural Resources Engineering, Luleå University of Technology, 2015.
a) *Section 1.*
b) *Section 3.1.*
c) *Section 3.2.*
d) *Section 5.1.*
e) *Section 5.4.*
f) *Section 7.2.*
g) *Section A.1.*
h) *Section A.2.*

[12] *SS 11 23 70. Utmattningsprovning - Metalliska material - Allmänna principer.* 2nd ed. MNC, METALLNORMCENTRALEN. SIS - Standardiseringskommissionen i Sverige. [In Swedish], 1978.
a) *Section 3.1.*
b) *Section 3.2.*

[13] M., Yafei et al. "Effects of Stress Ratio and Banded Microstructure on Fatigue Crack Growth Behavior of HRB400 Steel Bar". In: *Journal of Materials in Civil Engineering* 30.3 (2017), pp. 04017314-1-10.

[14] Zhu, M.L., Xuan, F.Z., and Tu, S.T. "Effect of Load Ratio on Fatigue Crack Growth in the Near-Threshold Regime: A Literature Review, and a Combined Crack Closure and Driving Force Approach". In: *Engineering Fracture Mechanics* 141 (2015), pp. 57–77. ISSN: 00137944.

[15] Suresh, S. *Fatigue of Materials.* 2nd ed. 1998. ISBN: 978-0-521-57847-9.
a) *Section 1.1.*
b) *Section 1.2.*
c) *Section 1.2.1.*
d) *Section 1.5.*
e) *Section 2.2.*
f) *Section 2.8.*
g) *Section 2.9.*
h) *Section 2.11.*
i) *Section 3.1.*
j) *Section 3.3.*
k) *Section 4.1.*
l) *Section 4.3.*
m) *Section 4.4.*
n) *Section 4.8.*
o) *Section 5.1.*
p) *Section 7.0.*
q) *Section 7.1.*
r) *Section 7.2.*
s) *Section 7.3.*
t) *Section 7.4.*
u) *Section 10.1.*

v) *Section 10.2.*
w) *Figure 2.2.*
x) *Figure 2.24.*
y) *Figure 10.2.*

[16] Yildirim, H.C. and Marquis, G.B. "Overview of Fatigue Data for High Frequency Mechanical Impact Treated Welded Joints". In: *Welding in the World* 56.7-8 (2012), pp. 82–96. ISSN: 00432288.

[17] Hobbacher, A. *Recommendations for Fatigue Design of Welded Joints and Components*. International Institute of Welding. 2008.
a) *Section 1.5.*
b) *Section 2.2.2.1.*
c) *Section 2.2.2.3.*
d) *Section 2.2.3.1.*
e) *Section 2.2.3.4.*
f) *Section 2.2.4.1.*
g) *Section 2.2.5.3.*
h) *Section 3.2.*

[18] Hull, D. and Bacon, D. J. *Introduction to Dislocations*. 5th ed. 2011. ISBN: 978-0-08-096672-4.
a) *Section 1.1.*
b) *Section 1.2.*
c) *Section 1.3.*
d) *Section 1.4.*
e) *Section 3.1.*
f) *Section 3.3.*
g) *Section 6.1.*
h) *Section 6.3.*
i) *Section 8.8.*
j) *Section 10.4.*
k) *Section 10.9.*
l) *Figure 1.5.*
m) *Figure 1.7.*
n) *Figure 1.10.*
o) *Figure 3.1.*
p) *Figure 3.4.*

[19] Zheng, H. and Abel, A.A. "Fatigue Properties of Reinforcing Steel Produced by TEMPCORE Process". In: *Journal of Materials in Civil Engineering* 11.2 (1999), p. 158. ISSN: 08991561.

[20] Rocha, M., Brühwiler, E., and Nussbaumer, A. "Geometrical and Material Characterization of Quenched and Self-Tempered Steel Reinforcement Bars". In: *Journal of Materials in Civil Engineering* 28.6 (2016), pp. 4016012-1 - 4016012-12. ISSN: 08991561.

[21] Rocha, M., Brühwiler, E., and Nussbaumer, A. "Microstructural Influence on the Scatter in the Fatigue Life of Steel Reinforcement bars". In: *International Journal of Fatigue* 75 (2015), pp. 205–212. ISSN: 0142-1123.

[22] fib, Bulletin 58. *Structural Concrete. Textbook on Behaviour, Design and Performance*. Tech. rep. CEB-FIP, 2010.
a) *Section 4.4.3.*

b) *Section 4.4.3.4.*

[23] Rocha, M., Brühwiler, E., and Nussbaumer, A. "Fatigue Behaviour Prediction of Steel Reinforcement Bars Using an Adapted Navarro and De Los Rios Model". In: *International Journal of Fatigue* 75 (2015), pp. 198–204. ISSN: 0142-1123.

[24] Majumdar, S. et al. "Optimum Rib Design in TMT Rebars to Enhance Fatigue Life While Retaining Bond Strength". In: *JOURNAL OF MATERIALS IN CIVIL ENGINEERING* 30.3 (2018). ISSN: 08991561.

[25] Rocha, M. et al. "Very High Cycle Fatigue Tests of Quenched and Self-Tempered Steel Reinforcement Bars". In: *Materials and Structures/Materiaux et Constructions* 49.5 (2016), pp. 1723–1732. ISSN: 13595997.

[26] Apostolopoulos, C.A. and Rodopoulos, C.A. "Inelastic Cyclic Behaviour of As-Received and Pre-Corroded S500s TEMCORE Steel Reinforcement". In: *International Journal of Structural Integrity* 1 (2010), p. 52. ISSN: 1757-9864.

[27] Taylor, D., Barrett, N., and Lucano, G. "Some New Methods for Predicting Fatigue in Welded Joints". In: *International Journal of Fatigue* 24.5 (2002), pp. 509–518. ISSN: 0142-1123.

[28] Tong, L. et al. "Experimental Study on Fatigue Behavior of Steel Reinforced Concrete (SRC) beams". In: *Engineering Structures* 123 (2016), pp. 247–262. ISSN: 0141-0296.

[29] Ma, Y. et al. "Static and Fatigue Behavior Investigation of Articial Notched steel Reinforcement." In: *Materials* 10.5 (2017). ISSN: 19961944.

[30] Amorn, W. et al. "Fatigue of Deformed Welded-Wire Reinforcement." In: *PCI JOURNAL* 52.1 (2007), pp. 106–122. ISSN: 08879672.

[31] Ayyub, B.M., Chang, P.C., and Al-Mutairi, N.A. "Welded Wire Fabric for Bridges. II: Fatigue Strength". In: *Journal of Structural Engineering (United States)* 120.6 (1994), pp. 1882–1892. ISSN: 0733-9445.

[32] Riva, P., Franchi, A., and Tabeni, D. "Welded Tempcore Reinforcement Behaviour for Seismic Applications". In: *Materials and Structures/Materiaux et Constructions* 34.238 (2001), pp. 240–247. ISSN: 1359-5997.

[33] Ohta, A., Maeda, Y., and Suzuki, N. "Residual Stress Effect on Fatigue Strength of Non-Load-Carrying Cruciform Welded Joints of SM570Q Steel For Welded structures." In: *Welding in the World* 46.11-12 (2002), pp. 20–25. ISSN: 00432288.

[34] *SS-EN 1993-1-9:2005. Eurocode 3: Design of Steel Structures - Part 1-9: Fatigue*. 1st ed. SSI - Swedish Standards Institute, 2005.
a) *Section 7.1.*
b) *Section 7.2.*

[35] Zong, L. et al. "Experimental and Numerical Investigation on Fatigue Performance of Non-Load-Carrying Fillet Welded Joints". In: *Journal of Constructional Steel Research* 130 (2017), pp. 193–201. ISSN: 0143-974X.

[36] Abdullah, E., Gotoh, K., and Deguchi, J. "Comprehensive Study of Structural Integrity of Non-Load-Carrying Fillet-Welded Joint Effect With Large Gap Size". In: *JOURNAL OF MARINE SCIENCE AND TECHNOLOGY* 20.4 (2015), pp. 752–764. ISSN: 09484280.

[37] Ahola, A., Nykänen, T., and Björk, T. "Effect of Loading Type on the Fatigue Strength of Asymmetric and Symmetric Transverse Non-Load Carrying Attachments." In: *FATIGUE FRACTURE OF ENGINEERING MATERIALS STRUCTURES* 40.5 (2017), pp. 670–682. ISSN: 8756758X.

[38] Lee, C.H. et al. "Effect of Weld Geometry on the Fatigue Life of Non-Load-Carrying Fillet Welded Cruciform Joints". In: *Engineering Failure Analysis* 16 (2009), pp. 849–855. ISSN: 1350-6307.

[39] Plos, M. et al. *Non-Linear Analysis and Remaining Fatigue Life of Reinforced Concrete Bridges. Background Document D4.5.* Tech. rep. Chalmers, CERVENKA, LTH, LTU, EPFL, SRA, 2007.
a) *Section 7.2.*
b) *Section 7.3.*

[40] Zilch, K. and Zehetmaier, G. *Bemessung im konstruktiven Betonbau.* In German. 2006. ISBN: 978-3-540-70637-3.

[41] *ISO 12107. Metallic Materials - Fatigue Testing - Statistical Planning and Analysis of Data.* 2nd ed. International Standard, 2012.

[42] Box, G. E. P., Hunter, J. S., and Hunter, W. G. *Statistics for Experimenters.* 2nd ed. 2005. ISBN: 0-471-71813-0.
a) *Section 2.5.*
b) *Section 3.2.*

[43] *SS-EN ISO 17660-2:2006, Welding - Welding of Reinforcing Steel - Part 2: Non Load-Bearing Welded Joints.* 1st ed. SSI - Swedish Standards Institute, 2006.
a) *Section 5.*
b) *Table 1.*
c) *Table 2.*

[44] Kopas, P. et al. "Fatigue Resistance of Reinforcing Steel Bars". In: *Procedia Engineering* 136.20 (2016), pp. 193–197. ISSN: 1877-7058.

[45] *SS-EN ISO 15630-2:2010. Steel for the Reinforcement and Prestressing of Concrete - Test Methods - Part 2: Welded Fabric.* 2nd ed. Section 8.4.7. SSI - Swedish Standards Institute, 2010.

[46] *SS-EN 1990. Eurocode - Basis of Structural Design.* 1st ed. SSI - Swedish Standards Institute, 2002.

Appendix A

Appendix

A.1 Additional Result Figures

Additional figures from the test results are presented here if details are interesting. A view of tested stress ranges in comparison to the entire S-N curves in EC2 [3a] is presented in Figure A.1, where it is difficult to interpret the result from the large scale. The idea is to show the experimental region as to stress ranges and corresponding fatigue life, in order to obtain a full overview of the tested region. Two magnifications of the test result, one for the stress range of 280 MPa and one for the three lower stress ranges is available, see Figure A.2 and Figure A.3.

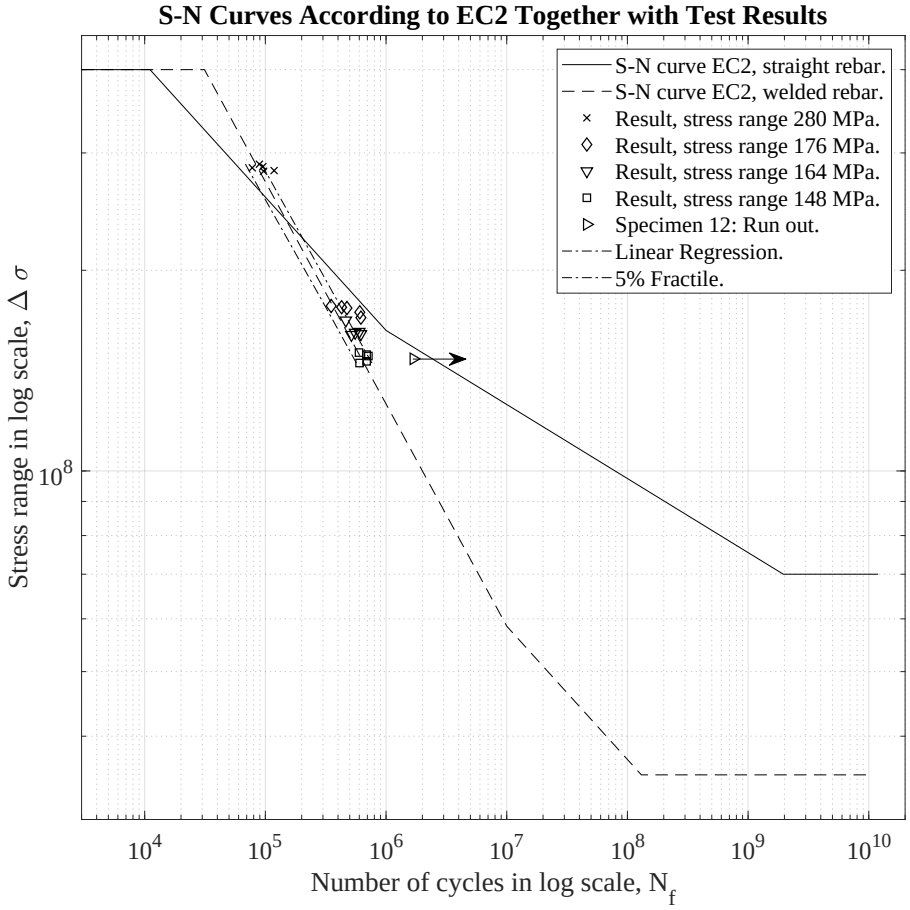

Figure A.1: S-N curves from EC2 together with test results. Linear regression curve and corresponding 5% fractile is also shown. A quite large scale in order to include the entire curve from EC2 [3c].

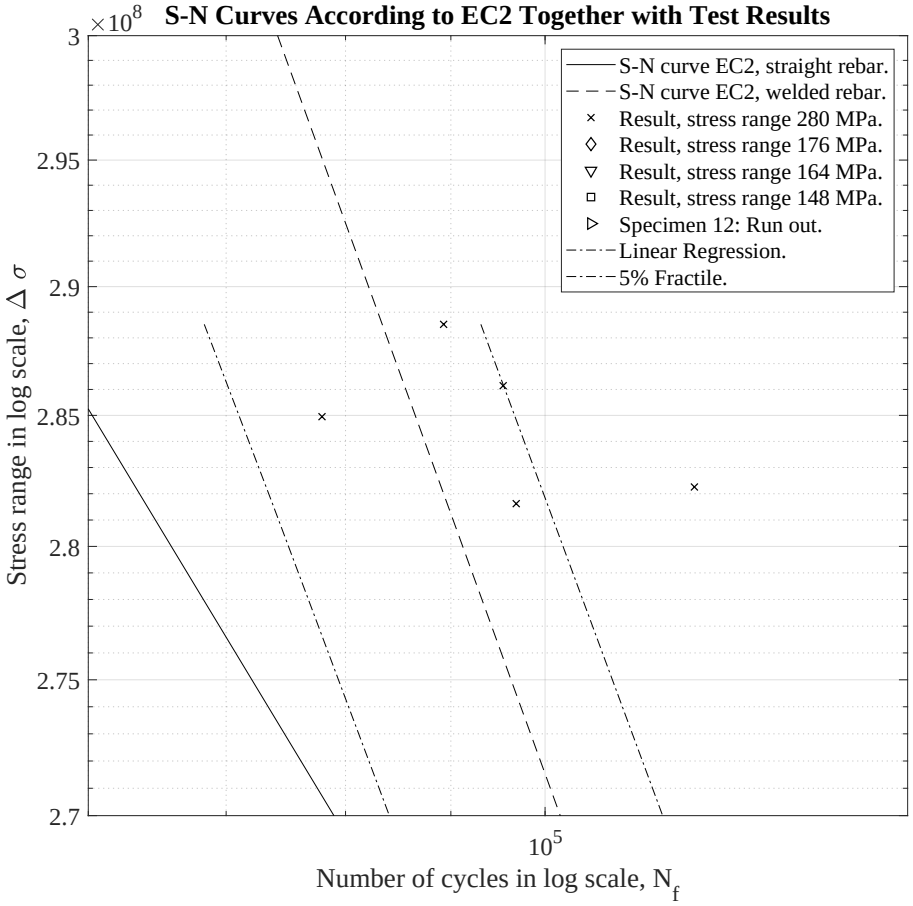

Figure A.2: S-N curves from EC2 together with test results. Linear regression curve and corresponding 5% fractile is also shown. Enlargement of 280 MPa stress range.

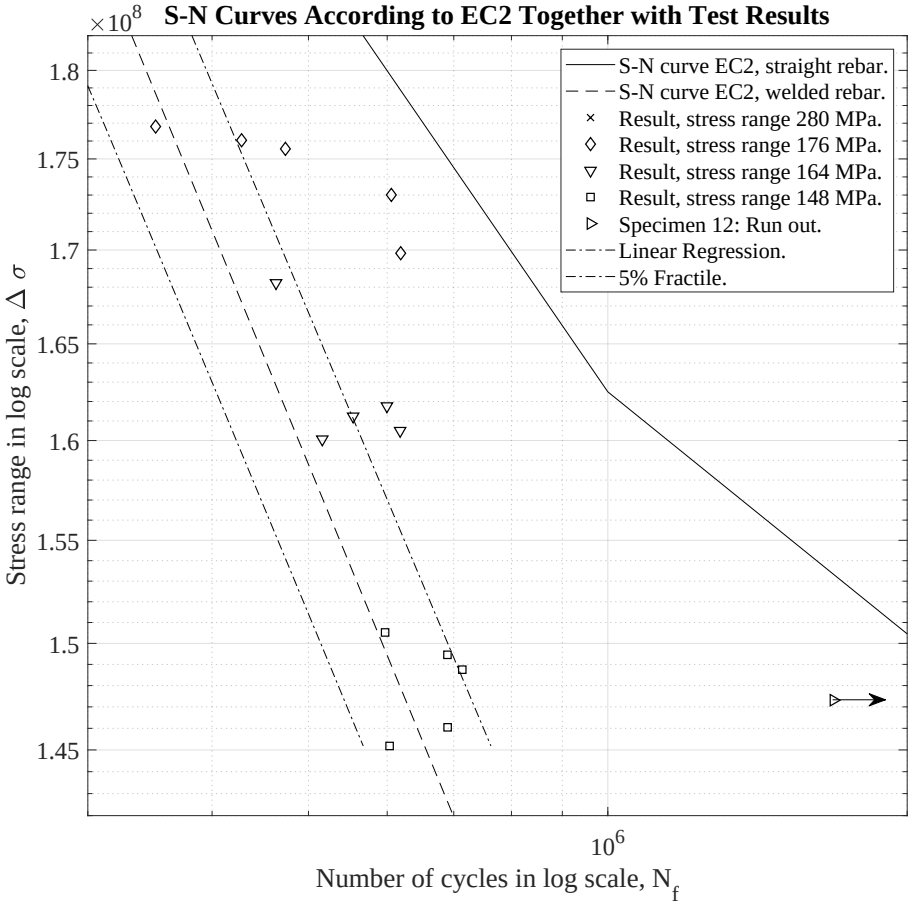

Figure A.3: S-N curves from EC2 together with test results. Linear regression curve and corresponding 5% fractile is also shown. Enlargement of the lower tested stress ranges, 176, 164 and 148 MPa.